AFCRL-66-755

AD642447

STUDY OF A MULTI-PULSE LASER RANGE FINDER

by

Sumner Ackerman
and
Thomas S. Morrison

EG&G, INC.
Crosby Drive, Bedford, Massachusetts

Contract No. AF 19(628)-5516

Project No. 7600

Task No. 760006

Scientific Report No. 2

Date of Report
20 October 1966

CLEARINGHOUSE FOR FEDERAL SCIENTIFIC AND TECHNICAL INFORMATION
Hardcopy $3.00 | Microfiche $.65 | 62 pp
ARCHIVE COPY
Code 1

DDC
NOV 30 1966

(CONTRACT MONITOR: Robert L. Illiff)

Distribution of this document is unlimited

Prepared

for

AIR FORCE CAMBRIDGE RESEARCH LABORATORIES
OFFICE OF AEROSPACE RESEARCH
UNITED STATES AIR FORCE
BEDFORD, MASSACHUSETTS

AFCRL-66-755

STUDY OF A MULTI-PULSE LASER RANGE FINDER

by

Sumner Ackerman
and
Thomas S. Morrison

EG&G, INC.
Crosby Drive, Bedford, Massachusetts

Contract No. AF 19(628)-5516

Project No. 7600

Task No. 760006

Scientific Report No. 2

Date of Report

20 October 1966

(CONTRACT MONITOR: Robert L. Illiff)

Distribution of this document is unlimited

Prepared

for

AIR FORCE CAMBRIDGE RESEARCH LABORATORIES
OFFICE OF AEROSPACE RESEARCH
UNITED STATES AIR FORCE
BEDFORD, MASSACHUSETTS

ABSTRACT

A programmed multi-pulse optical radar range finder is analyzed. An experimental multi-pulse laser has been developed and its characteristics are described.

If the target is optically "smooth", or is well resolved by the receiver, the multi-pulse range finder has an effective power gain slightly less than its output energy gain when the noise level is low and the detection probability is high. The useful energy gain of a ruby laser due to multi-pulsing was experimentally measured as about 8 dB.

Under the conditions of geodetic satellite ranging, the target is generally optically "rough" in the extreme; then the multi-pulse range finder has a power gain of from 10 dB to over 25 dB, depending on the relative transmitter efficiencies and the acceptable detection probability. This significant increase in the advantage of the multi-pulse system results from the detection statistics that are valid when signal scintillation due to the target is present.

LIST OF CONTRIBUTORS

Sumner Ackerman, Scientific Specialist, EG&G, Inc., Bedford, Mass.

William G. Madison, Senior Scientist, EG&G, Inc., Bedford, Mass.

Thomas S. Morrison, Senior Engineer, EG&G, Inc., Bedford, Mass.

RELATED CONTRACTS AND PUBLICATIONS

PREVIOUS OR RELATED CONTRACTS

1. Contract No. AF 19(628)-2950 (Experimental Geodetic Laser System)

2. Contract No. AF 19(628)-5516 (Design Study of Advanced Geodetic Laser System)

PREVIOUSLY PRODUCED OR PROJECTED PUBLICATIONS

1. Ackerman, Sumner, "High Energy Laser System for Geodetic Research," Final Report, AFCRL No. 65-671, 30 Sept. 1965 (Contract No. AF 19(628)-2950.

2. Ziffer, G.F., and Maxwell, J.P., "Control Unit for Advanced Geodetic Laser System," Report No. B-3364, EG&G, Inc., Bedford, Mass., 11 August 1966.

3. Ackerman, Sumner, "Design Study of Advanced Geodetic Laser System," AFCRL Scientific Report No. 1, 30 Sept. 1966, (Contract No. AF 19(628)-5516, Item 3).

4. Ackerman, Sumner, "Threshold Detection of Geodetic Satellite Images," AFCRL Scientific Report No. 3 (to be published) (Contract No. AF 19(628)-5516, Item 1).

5. Ackerman, S., Morrison, T.S.. and Iliff, R.L., "A Programmed Multi-Pulse Range Measurement System," Journal of Applied Optics (to be published).

TABLE OF CONTENTS

LIST OF ILLUSTRATIONS

LIST OF TABLES

SECTION 1

INTRODUCTION

1.1 PURPOSE

The work described in this report is directed toward improving the performance of pulsed ruby lasers used to measure the range of geodetic satellites over distances that are often greater than 1000 km Two characteristics of ruby lasers which singularly impair or restrict their range measurement capabilities are: (1) a very low Q-switched mode efficiency, generally about 0.1%; and (2) a susceptibility to damage at high peak-power outputs of the magnitude 10^9 watts. It had been anticipated that both of these limitations could be significantly lessened by programmed multi-pulsing of the laser, that is, by generating several giant pulses at precisely timed intervals during a single pumping period. Efficiency should be improved by depleting the inverted population at relatively short intervals so that incoherent fluorescence losses are minimized. The peak power required for a given range should be reduced, since each of the multiple output pulses would have equal or less energy than a single pulse

The only known analysis that compares multi-pulse and single-pulse systems, prior to the work described herein, is based on a Gaussian model approximation of the noise statistics wherein the rms value of the average noise energy, $\bar{N}_s$,* is equal to $\sqrt{\bar{N}_s}$. In this situation, the signal energy (or power) is increased by MK for M pulses of magnitude K times a single pulse, and the rms noise is increased by $\sqrt{M}$ due to the M samplings. The net energy gain for a given signal-to-noise ratio is then $K\sqrt{M}$. This approximate model may be reasonably accurate when $\bar{N}_s > 20$, but it is not satisfactory if the noise level is relatively small, i.e., $\bar{N}_s < 1$, or when Gaussian statistics alone are not applicable at any noise level. Both of these conditions are of particular interest.

1.2 SCOPE

This report summarizes the work performed by EG&G, Inc., under Contract AF 19(628)-5516, Item 2. This item includes a "...theoretical and experimental satellite laser ranging study to determine the feasibility

---

*Averaged over the sampling time, which is generally equal to the signal pulse duration.

of generating and using several (optimum number to be determined) precisely controlled pulses in order to code the laser output for signal identification. The receiver (study only) shall accept only pulses in the preselected code, thereby eliminating the requirement that the signal return must exceed the noise. This technique shall allow less peak power for a given range without increasing the "false-alarm" or "no-range" probability. This study shall include, but shall not necessarily be limited to, the following:

(1) Study of maximum peak power and energy output for a sequentially Q-switched laser oscillator; one to many output pulses in approximately 10^{-3} second pump period.

(2) Study of signal-processing methods to optimize accuracy and reliability of range measurements.

(3) Theoretical and experimental determination of typical noise conditions.

(4) Experimental determination of the optimum pulse length and pulse spacing compatible with current laser technology for ranging identification."

In the performance of this task, an analysis of the multi-pulse range finder was made, assuming the Poisson probability distribution of signal and noise that is applicable to specular targets and the negative-binomial signal statistics applicable to optically "rough" targets.* The single-pulse system was treated as a special case (M = 1) for comparison. This work is described in Section 2 of this report. An experimental multi-pulse range finder and results of experimental noise measurements are described in Section 3.

*Goodman, J.W., "Some Effects of Target-Induced Scintillation on Optical Radar Performance," Proc. IEEE, 53, November 1965, 1688-1700.

SECTION 2

THEORETICAL STUDY

2.1 FUNCTIONAL MODEL OF A MULTI-PULSE RANGE FINDER

Figure 1 is a functional diagram of a multi-pulse range finder. The modulator of an electro-optical (Q-switch) shutter is triggered with a series of M pulses which are developed by a digital-clock-controlled programmer. The modulator output pulses are spaced so that the M number of Q switched laser pulses generated during each pumping period have approximately the same energy and waveshape. In the elementary oscilloscope-detection method illustrated, the M pulses are precisely delayed for a period equal to the estimated minimum range time. The delayed M pulses (D pulses) trigger the range oscilloscope sweep which has a time duration T, equal to the time interval in which the range is in doubt. During the period between D pulses, the oscilloscope beam is caused to move vertically by an appropriate increment so that the range detector output is displayed as shown in Fig. 2. If various pulse-delay uncertainties (jitter) are less than the resolvable time interval τ, and the received signal pulse duration is $\leq \tau$, the intervals τ which can contain both signal and noise are in a single column of the display ensemble consisting of M (T/τ) elements; elements that can have only noise energy are randomly distributed.

It will become evident from the following analysis that this choice of functional model is convenient and does not restrict the generality of the results. As a practical matter, this multi-pulse detection method is relatively simple and inexpensive, particularly when the D pulses are synchronously delayed reproductions of the M pulses; it is capable of range accuracies to less than 10 meters if T is not more than a few microseconds and T/τ is equal to or less than approximately 200.

2.2 DETECTION ANALYSIS FOR RESOLVED AND SPECULAR TARGETS

It has been established, theoretically and experimentally, that photoemission is accurately described by Poisson statistics.* When the

*Mandel, L., "Fluctuations of Photon Beams; The Distribution of Photoelectrons", Proc. Phys. Soc. (London), 74, No. 475, 1959.

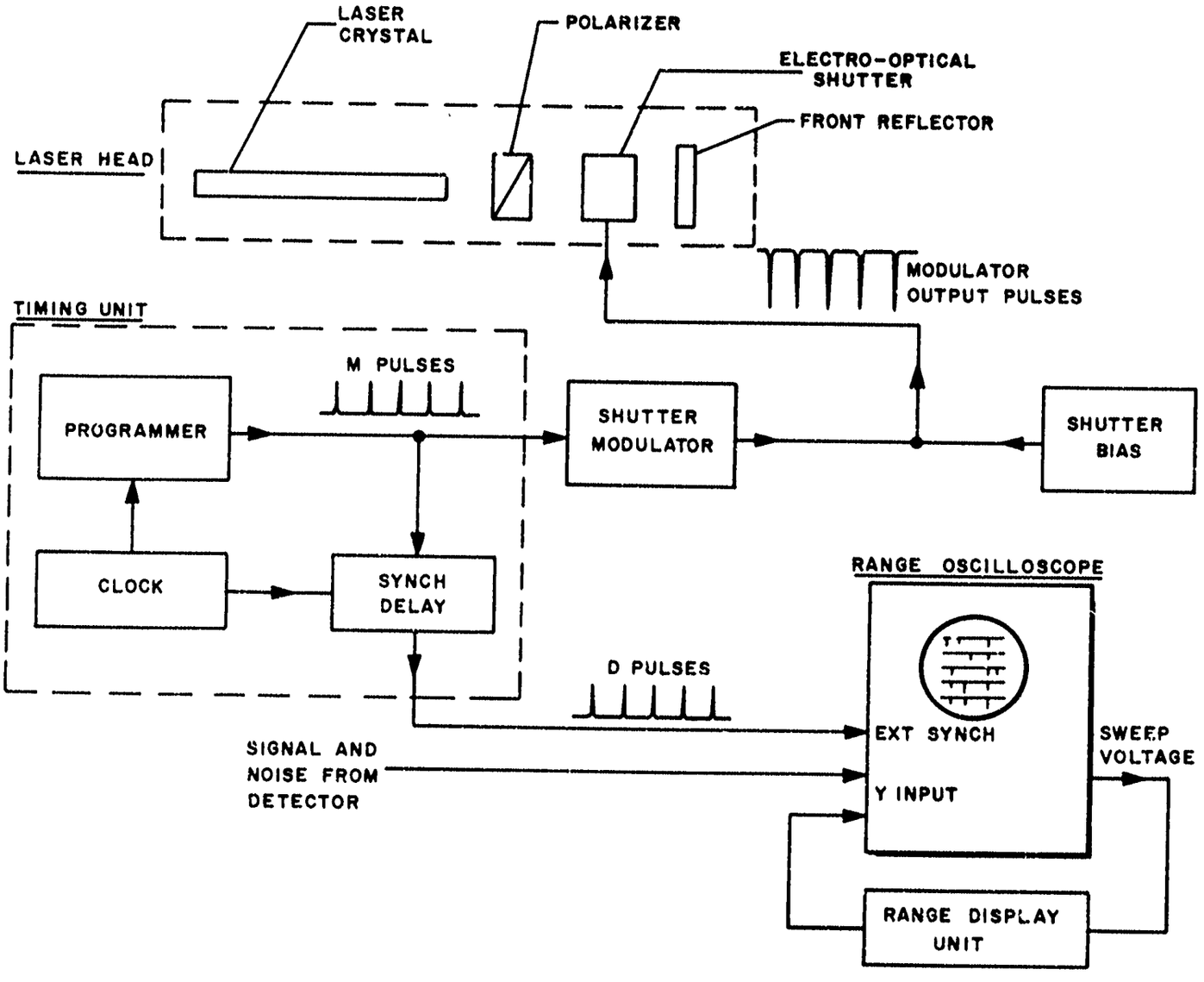

Fig. 1. Functional diagram of a multi-pulse laser range finder.

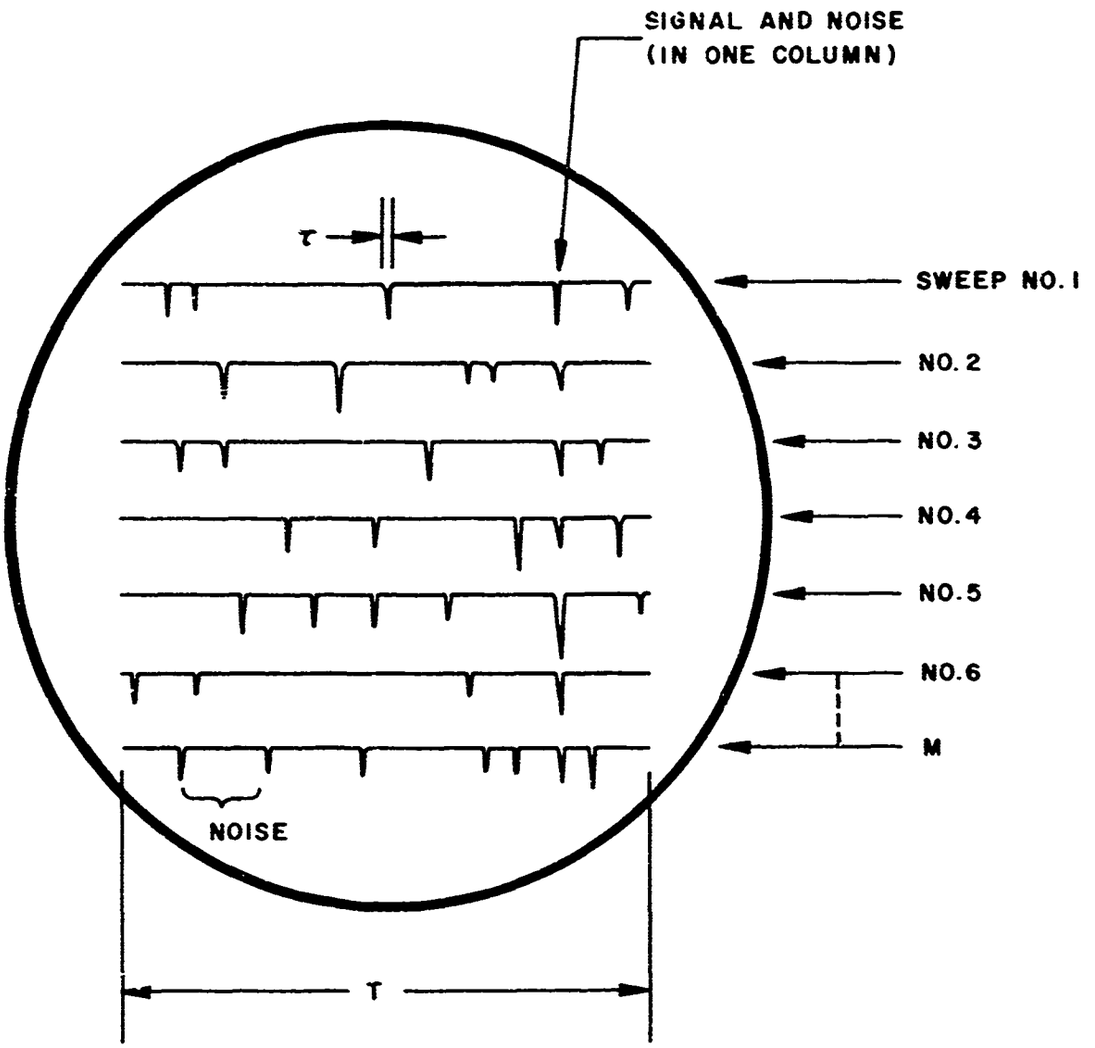

Fig. 2. Range data display of multi-pulse laser range finder.

incident energy on the photodetector is known, by measurement or in principle, the probability that S or more photoelectrons will be emitted by the detector can be evaluated as

$$P(S) = \sum_{X=S}^{\infty} \frac{\bar{N}^X}{X!} \exp\left[-N\right] \tag{1}$$

where

$$\bar{N} = J\eta \tag{2}$$

is the average number of photoelectrons emitted, J is the incident energy in number of photons, and η is the quantum efficiency of the detector.

Background illumination, the principal source of noise under nighttime satellite ranging conditions, is readily measured.* Then, the probability of S or more photoelectrons due to noise in the interval τ is

$$P(S_\tau) = \sum_{X=S}^{\infty} \frac{\bar{N}_n}{X!} \exp\left[-\bar{N}_n\right] \tag{3}$$

where $\bar{N}_n$ is the average noise photoelectron count in the interval τ; and the probability of S or more noise photoelectrons during the range observation time, T, is

$$P(S_T) = 1 - \left[1 - P(S_\tau)\right]^{(T/\tau - 1)} \tag{4a}$$

or

$$P(S_T) \simeq (T/\tau - 1)\left[P(S_\tau)\right], \qquad \begin{array}{l} T > \tau \\ P(S_\tau) <<< 1 \\ P(S_T) << 1 \end{array} \tag{4b}$$

T is the interval over which the predicted range is in doubt.

---

*Section 3.3.

If the target is optically "smooth" (specular), such as an optical flat or a single precise cube corner, or if it is well resolved by the receiver,* the received signal energy can, in principle, be predicted and the probability of S or more photoelectrons in the interval τ is

$$P(S_s) = \sum_{X=S}^{\infty} \frac{(\bar{N}_s + \bar{N}_n)^X}{X!} \exp\left[-(\bar{N}_s + \bar{N}_n)\right] \tag{5}$$

$\bar{N}_s$ is the average number of signal photoelectrons during the interval τ.

When statistically independent random functions which have a Poisson distribution are added, their sum will be a random function with the same distribution. It follows that photoelectrons emitted in any group of discrete intervals of τ in the display ensemble (Fig. 2) may be added, and the resulting random function is described by Poisson statistics. Therefore, the probability of S or more photoelectrons being emitted in one or more of the $(T/\tau - 1)$ columns of $M\tau$ intervals which have only noise energy is

$$P(FA) = 1 - \left[1 - \sum_{X=S}^{\infty} \frac{(M\bar{N}_n)^X}{X!} \exp\left[-M\bar{N}_n\right]\right]^{(T/\tau - 1)}, \qquad M \geq 1 \tag{6a}$$

or

$$P(FA) \approx (T/\tau - 1) \sum_{X=S}^{\infty} \frac{(M\bar{N}_n)^X}{X!} \exp\left[-M\bar{N}_n\right], \tag{6b}$$

$$M \geq 1$$
$$P(FA) << 1$$

*For example, if the individual cube corners in an array can be resolved.

The probability of S or more photoelectrons in the one column of M τ elements that contains signal and noise is

$$P(D) = \sum_{X=S}^{\infty} \frac{\left[M(\bar{N}_s + \bar{N}_n)\right]^X}{X!} \exp\left[-M(\bar{N}_s + \bar{N}_n)\right], \quad M \geq 1 \qquad (7)^*$$

The value of S in Equation 6 must be such that for a given magnitude of noise, $M\bar{N}_s$, P (FA) will be acceptably small; S is commonly called the receiver "threshold" and P (FA) is the probability of ambiguity, or one or more "false alarms". The magnitude of $M(\bar{N}_s + \bar{N}_n)$ in Equation 7 must be such that, for the same value of S, P (D) is acceptably close to unity; P (D) is the probability of signal detection.** Note that Equations 6 and 7 apply either to the multi-pulse range finder or the single-pulse system, where M = 1.

---

*Note that the parameter $M(\bar{N}_s + \bar{N}_n)$ in this equation can be expressed more generally as

$$\sum_{j=1}^{M} (\bar{N}_s)_j + M\bar{N}_n$$

That is, the total average signal energy due to M transmitted pulses is important; it is not necessary that the transmitted pulses be equal in energy or have any particular relationship. If the energy per pulse is not transferable, it is desirable, of course, to have a significant amount of signal energy in each of the M pulses, since noise energy is also being summed M times.

**The probabilities P (FA) and P (D) are neither statistically independent or mutually exclusive; for these reasons a single figure of merit for detection cannot be evaluated in a reasonably simple manner. A figure of merit such as "signal/noise ratio" is meaningful under high background noise conditions, when N > 20 and the approximation of a Gaussian distribution is valid.

Solutions to Equations 6 and 7 have been computed with the aid of Poisson distribution tables* over a range of average noise levels from $\bar{N}_n = 0$ to $\bar{N}_n = 10$. P (FA) can be normalized with respect to the number of intervals τ in a range observation period T, so that

$$P(FA) \simeq \frac{T}{\tau} P(fa) \qquad (8)$$

P (fa) is kept close to 10^{-5} in the results tabulated in Table 1 and plotted in Fig. 3.

Table 1. Comparison of single- and multi-pulse detection for specular and resolved targets (m = ∞).

$\bar{N}_n$	S_7	S_1	$\bar{N}_{s7}$	$\bar{N}_{s1}$	$R = \bar{N}_{s1}/\bar{N}_{s7}$
0	1	1	1	7	7
0.01	4	3	1.77	11	6.3
0.05	6	4	2.31	13	5.6
0.10	7	5	2.65	14	5.3
0.50	15	7	3.75	17.5	4.7
1.0	22	8	4.64	19.5	4.2
5.0	64	17	6.70	24.5	3.7
10.0	109	27	10.6	36	3.4

$P(fa) \leq 10^{-5}$ $\qquad$ $P(D) \simeq 0.9990$

S_7 ≡ Threshold for multi-pulse radar (M = 7), in number of photoelectrons.

S_1 ≡ Threshold for single-pulse radar (M = 1), in number of photoelectrons.

$\bar{N}_{s7}$ ≡ Average signal per pulse required, in number of photoelectrons, when M = 7.

$\bar{N}_{s1}$ ≡ Average signal energy required, in number of photoelectrons, when M = 1.

*General Electric Co., Defense Systems Dept., Tables of the Individual and Cumulative Terms of Poisson Distribution, D. Van Nostrand Co., Inc., Princeton, N.J.

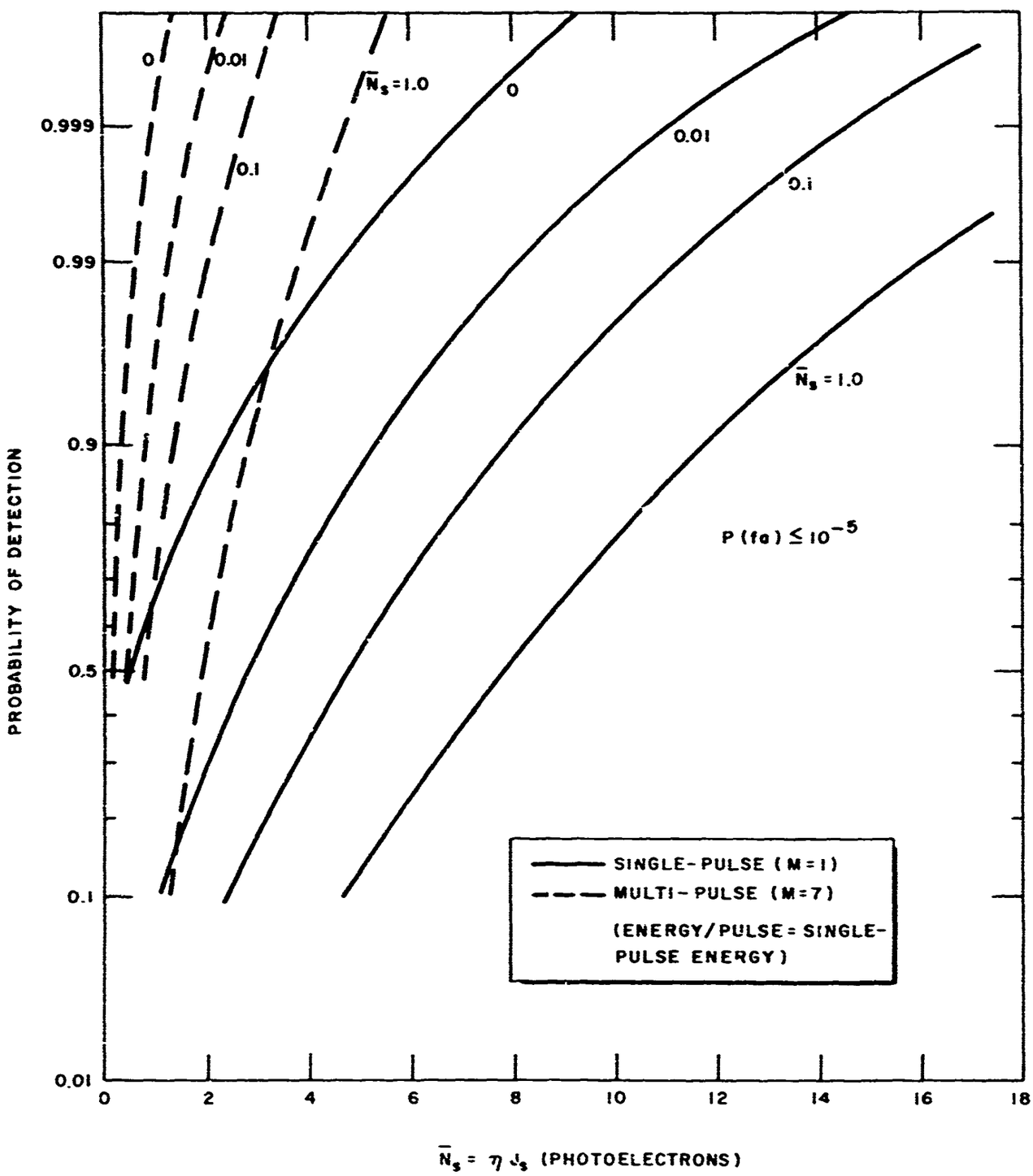

Fig. 3. Comparison of single- and multi-pulse detection for specular and resolved targets.

A few interesting aspects of the results are quickly apparent. Note that the "power advantage ratio," $R = \bar{N}_{S1}/\bar{N}_{S7}$, is equal to M when $\bar{N}_n = 0$, and diminishes steadily as $\bar{N}_n$ increases. This is a consequence of having to multiply the noise in each element τ by M in Equation 6; it is evident that splitting a given amount of energy into M parts is actually a disadvantage when $\bar{N}_n > 0$. For the tabulated values of R to be valid, the energy (and peak power) of each of the M pulses must be equal to that of the single pulse; the value of R changes proportionally to the extent this condition is not met. Apparently R is approaching $\sqrt{M}$ as $\bar{N}_n$ gets large, as predicted in paragraph 1.1.

It should be noted that the division of the data display ensemble into discrete intervals, τ, excludes an analytical evaluation of range resolution within this period of time. Actually, τ may be about 30 nanoseconds which is equivalent to less than 5 meters of range. This is not a significant limitation, considering the geodetic satellite ranges are of magnitude 1000 km and an acceptable range error is ±10 meters; the simplifying assumption of discrete observation cells is well justified under such conditions.

2.3 DETECTION ANALYSIS FOR OPTICALLY ROUGH TARGETS

It has been shown* that when the target is optically rough and is not well resolved by the receiver, the receiving aperture intercepts some number, $m \geq 1$, of spacial correlation cells into which the reflected energy is distributed. Each correlation cell is a statistically independent random function of the reflected signal energy (Bose-Einstein distribution) whose average value is the signal energy that would be expected if the target were specular. The magnitude of m is determined by the transmitter wavelength and the ranging system geometry (see page 12). In general, signal plus noise detection is described by a negative binomial distribution, so that the probability of S photoelectrons due to signal and noise is (for a single pulse)

$$P(S_r) = \left(\frac{m}{m + \bar{N}_s}\right)^m \frac{\exp(-\bar{N}_n)}{m-1} \sum_{X=0}^{S} \frac{(S + m - X - 1)!}{X!\,(S - X)!} (\bar{N}_n)^X \left(\frac{\bar{N}_s}{m + \bar{N}_s}\right)^{S-X} \qquad (9)$$

*Goodman, J. W., op cit, p. 2. In Goodman's notation: $m \longrightarrow M$ $S \longrightarrow k$ $X \longrightarrow j$ $L \longrightarrow R$

and the probability of S or more photoelectrons (detection probability) is

$$P(D_r) = \sum_{X=S}^{\infty} P(S_r) \qquad (10)$$

Noise due to background illumination is accurately described by the Poisson distribution, as before, so that

$$P(fa) = \sum_{X=S}^{\infty} \frac{(M\bar{N}_n)^X}{X!} \exp\left[-M\bar{N}_n\right], \qquad M \geq 1 \qquad (11)$$

See paragraph 2.2

In the extreme case of target roughness , when the receiving aperture intercepts only one correlation cell (m = 1), the negative-binomial distribution reduces to Bose-Einstein statistics and (for a single pulse)

$$P(S_r) = \frac{\exp\left[-\bar{N}_n\right]}{1 + \bar{N}_s} \sum_{X=0}^{S} \frac{\bar{N}_n^X}{X!} \left(\frac{\bar{N}_s}{1 + \bar{N}_s}\right)^{S-X}, \qquad m = 1 \qquad (12)$$

on

At the other extreme, when m = ∞, the receiver intercepts all the spacial correlation cells , Equation 9 reverts to the Poisson distribution, and the analysis in paragraph 2.2 for signal plus noise detection is valid.* Goodman has formulated an approximate calculation for m based on geometric parameters of the ranging situation,

$$m = \left[2\int_0^1 (1-y)\ \mathrm{sinc}^2\ \frac{l_o l_r y}{\lambda L}\ dy\right]^{-2} \qquad (13)$$

*Evaluations of Equation 9 show that the Poisson distribution is reasonably accurate when m ≥ 10.

l_o and l_r are the widths of square target and receiver apertures, λ is the transmitter wavelength, and L is the range. The solution of Equation 13 is plotted in the cited paper, and in Fig. 4, for m vs the normalized range:

$$\frac{\lambda L}{\pi l_o l_r}$$

Representative geodetic satellite ranging parameters are:

$L = 10^6$ meters,

$\lambda = 0.69 \times 10^{-6}$ meters,

$l_o = 0.2$ meters,

$l_r = 0.2$ meters

For these values, the normalized range is 5.5 and m = 1. Therefore, Equation 12, the Bose-Einstein detection statistics, is of principal interest.

Detection statistics based on the Bose-Einstein distribution has been generalized to include the multi-pulse case; this is described in some detail in Appendix A. The mixing of noise with the signal was neglected ($\bar{N}_n$ assumed = 0); under these conditions,

$$P\left[D_{1\,M0}\right] = \sum_{X=S}^{\infty} \binom{-M}{S} \left(\frac{1}{1+\bar{N}_s}\right)^M \left(-\frac{\bar{N}_s}{1+\bar{N}_s}\right)^X \qquad (14)$$

$$M \geq 1$$
$$\bar{N}_n = 0$$

$$\binom{-M}{S} = \frac{(-M)(-M-1)\cdots(-M-S+1)}{S!}$$

$$\binom{-M}{0} = 1, \text{ by definition.}$$

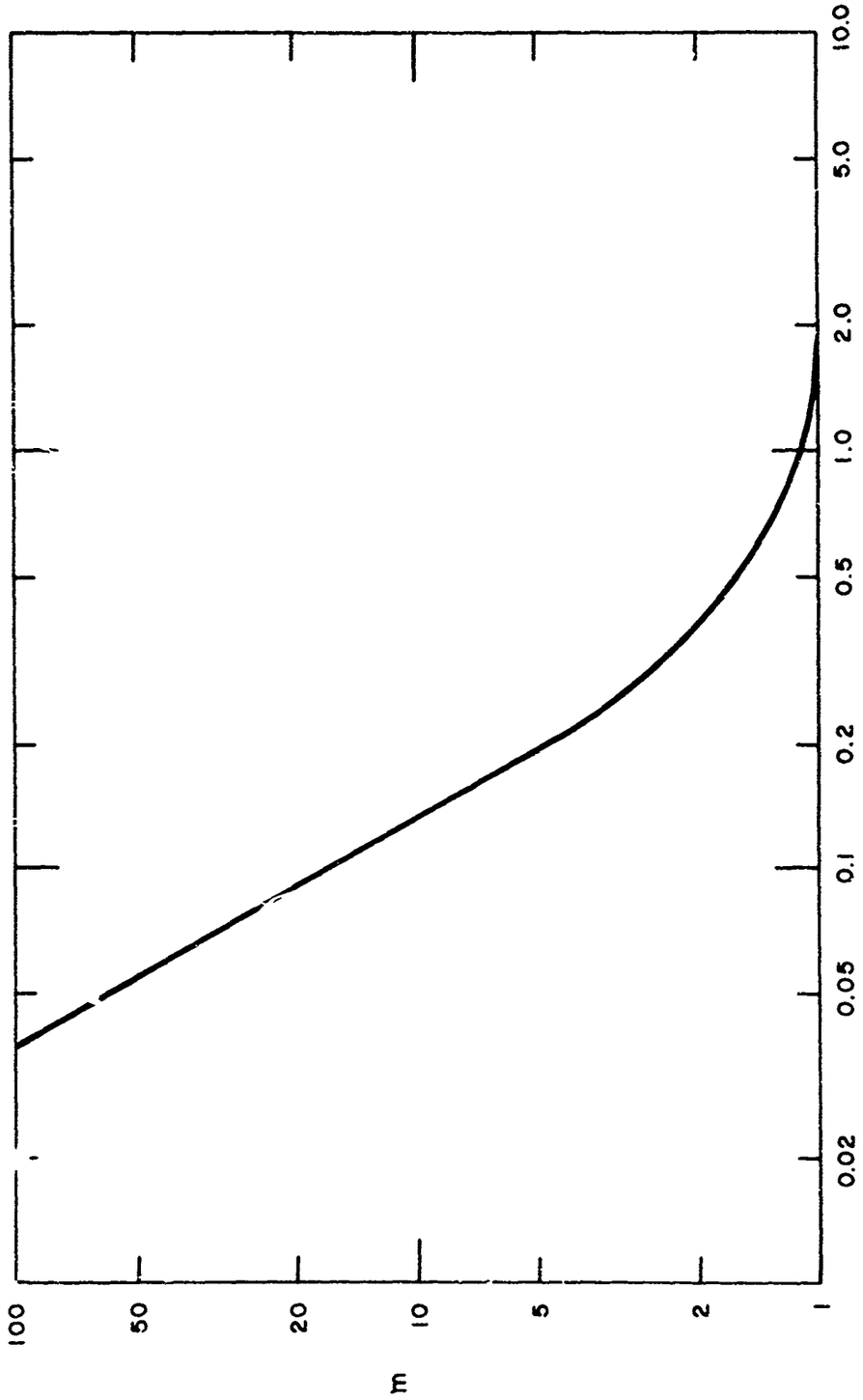

Fig. 4. m as a function of range system geometry.

The subscript 1 M0 indicates the event detection for m = 1, M pulses. and 0 noise. Equation 14 is a good approximation when $\bar{N}_n < 1$ (nighttime operation) and gives a conservative result with respect to multi-pulse performance at any finite value of noise.

Equations 11 and 14 have been evaluated for a few conditions of special interest.* These results are summarized in Table 2. They show a considerable advantage for the multi-pulse technique, particularly when the probability of detection is high. The difference between the multi-pulse and single-pulse systems is evidently affected much more by the probability of detection than by the noise level; this is in contrast to the situation when Poisson statistics are valid.

Before concluding this section, it should be noted that this analysis is concerned with the phenomenon of target scintillation and does not consider the effect of atmospheric scintillation; these results, then, are only valid when the atmospheric influence on signal statistics is small by comparison. Other assumptions concerning the polarization, spectral, and temporal characteristics of the transmitter appear to be valid for the type of equipment that is generally used for satellite range finding.

2.4 SUMMARY AND DISCUSSION OF ANALYTICAL RESULTS

When the target is optically smooth, or is well resolved by the receiver, the multi-pulse ruby laser range finder has an energy (or power) advantage over the same range finder when single-pulsed. This advantage is a consequence only of the additional energy output that can be obtained from the laser transmitter by multi-pulsing. It amounts to approximately a 7 to 8 dB power gain, based on the experimental results discussed in Section 3, and assuming typical nighttime background illumination levels.

Under the usual conditions of geodetic satellite ranging, where range distances are large and the target reflector consists of assemblies of numerous small cube corners, detection must be considered in the presence of target scintillation. The target is optically rough in the extreme, and only one of many spacially distributed signal correlation

*The evaluation of Equation 14 involves the solution of very high-order quadratic equations as $\bar{N}_n$, and therefore S, becomes large. The results for $\bar{N}_n = 0.05$ and 0.1 were obtained with an electronic computer.

Table 2. Comparison of single- and multi-pulse detection for optically rough targets (m = 1).

$\bar{N}_n$	$P(D_r)$	S_7	S_1	$\bar{N}_{s7}$	$\bar{N}_{s1}$	R
0	0.999	1	1	1.68	999	595
0	0.990	1	1	0.93	99	10^6
0	0.970	1	1	0.65	32.3	49.7
0.01	0.999	4	3	3.89	2,998	771
0.01	0.990	4	3	2.37	298	125
0.01	0.970	4	3	1.79	98	54.7
0.05	0.999	6	4	5.26	3,998	760
0.05	0.990	6	4	3.26	397.5	122
0.05	0.970	6	4	2.50	130.5	52.2
0.10	0.999	7	4	5.93	3,998	674
0.10	0.990	7	4	3.70	397.5	107
0.10	0.970	7	4	2.85	130.5	45.7

$P(fa) \leq 10^{-5}$

$P(D_r) \equiv$ Probability of detection, rough target (m = 1). See Table 1 for definition of other terms.

cells is intercepted by the receiver aperture. The statistics of signal detection are then markedly changed, and the average signal energy required for a single-pulse measurement may be 1 to 3 orders of magnitude greater for a given detection probability of let us say greater than 0.970, than when target scintillation is not present (Table 2). A multi-pulse system, with M = 7, requires only a doubling of signal energy for a detection probability of 0.9990, and less than this at lower probabilities. Under these conditions, the multi-pulse range finder may have a power advantage of from 15 dB to over 28 dB, depending on the acceptable detection performance and assuming it has 8 dB more energy output. Evidently there will be a significant advantage for the multi-pulse system,

even if its total energy output is less than that of the single-pulse range finder. A number of statistically independent observations per range event is particularly advantageous in the presence of target scintillation.

The rough target phenomenon can explain a number of otherwise anomalous experimental results. For example, when geodetic satellite range measurements are made with a laser operating in the normal mode, or with a randomly multi-pulsing Q-switched laser, there is generally little correlation in the magnitudes of corresponding transmitted and received pulses. Lehr and associates have reported that actual returned signal energy was 20 dB less than expected in a number of satellite ranging experiments. * This is in reasonably good agreement with what the target scintillation theory predicts, if unambiguous detection probability during these observations was approximately 0.970 under low background noise conditions. Judging from the limited data available on the returned signal photons and the noise, it appears possible that this was the circumstance during many of the experiments reported.

The average received energy per pulse required for a desired detection performance, $\bar{N}_{sm}$, can be computed from Equations 11 and 14 for cases where $m = 1$, $M \geq 1$, and $\bar{N}_n < 1$; these equations have been evaluated for a limited number of conditions and the results appear in Table 2. $\bar{N}_{sm}$ can be divided by the quantum efficiency of the photodetector to determine the required energy per pulse in photons. The necessary transmitted energy is then computed from the range equation, making appropriate allowances for systematic and measurable (in principle) phenomena such as velocity aberration, which may not be considered in the equation. **

The theory of signal detection in the presence of target scintillation will be extended to include photographic detection with a normal-mode laser illuminator in AFCRL Scientific Report No. 3 (Contract No. AF19(628)-5516), to be published shortly.

---

*Lehr, C.G., Maestre, L.A., and Anderson, P.H., "Measurements of Satellite Range with a Ruby Laser," Special Report No. 211, Smithsonian Inst. Astrophys. Obs., May, 1966.

**AFCRL Scientific Report No. 1 (Contract No. AF19(628)-5516).

SECTION 3

EXPERIMENTAL STUDY

3.1 DESCRIPTION OF EXPERIMENTAL MULTI-PULSE LASER (EML)

Figures 5 thru 7 are photographs of the EML head, which is largely of conventional design and which comprises the following major components:

(1) Crystal - 60° Ruby, 0.05% Cr concentration by weight. 1/2-in. diameter x 6 in. long. Plane ends, flat to $\lambda/10$ and parallel within 2 arc-seconds. Back coating for 99.9% reflectance at 6943Å. Front coating for 0.002% reflectance at 6943Å. Body surface polished, ground.*

(2) Flashtube - EG&G Type FX-81-6B (See Fig. 8.)

(3) Pump reflectors - Cylindrical (split). 3-1/4-in. ID. 0.010-in. thick silver plate, over 5 micro-in. surface finish.

(4) Q-switch shutter - 25 x 15-mm aperture Kerr cell.

(5) Q-switch polarizer - 15 x 15-mm aperture Glan-Thomson prism.

(6) Front mirror** - (2) Quartz etalons, or (2) sapphire etalons, or (1) multi-layer dielectric reflector, 50% reflectance at 6943Å.

The integral flashtube-anode connector design (Fig. 9), and a front mirror support (Fig. 10) that uses a spherical bearing to achieve stability and ease of adjustment are the only features of the EML head

*Both types of crystal body finish have been used; no significant difference in performance that can be attributed to crystal-surface finish has been observed.

**Optimum front mirror reflection depends on crystal, if cavity losses per pass, cavity, geometry, and pulse shape remain constant; measurements on this laser indicated the value of this reflection is not very critical.

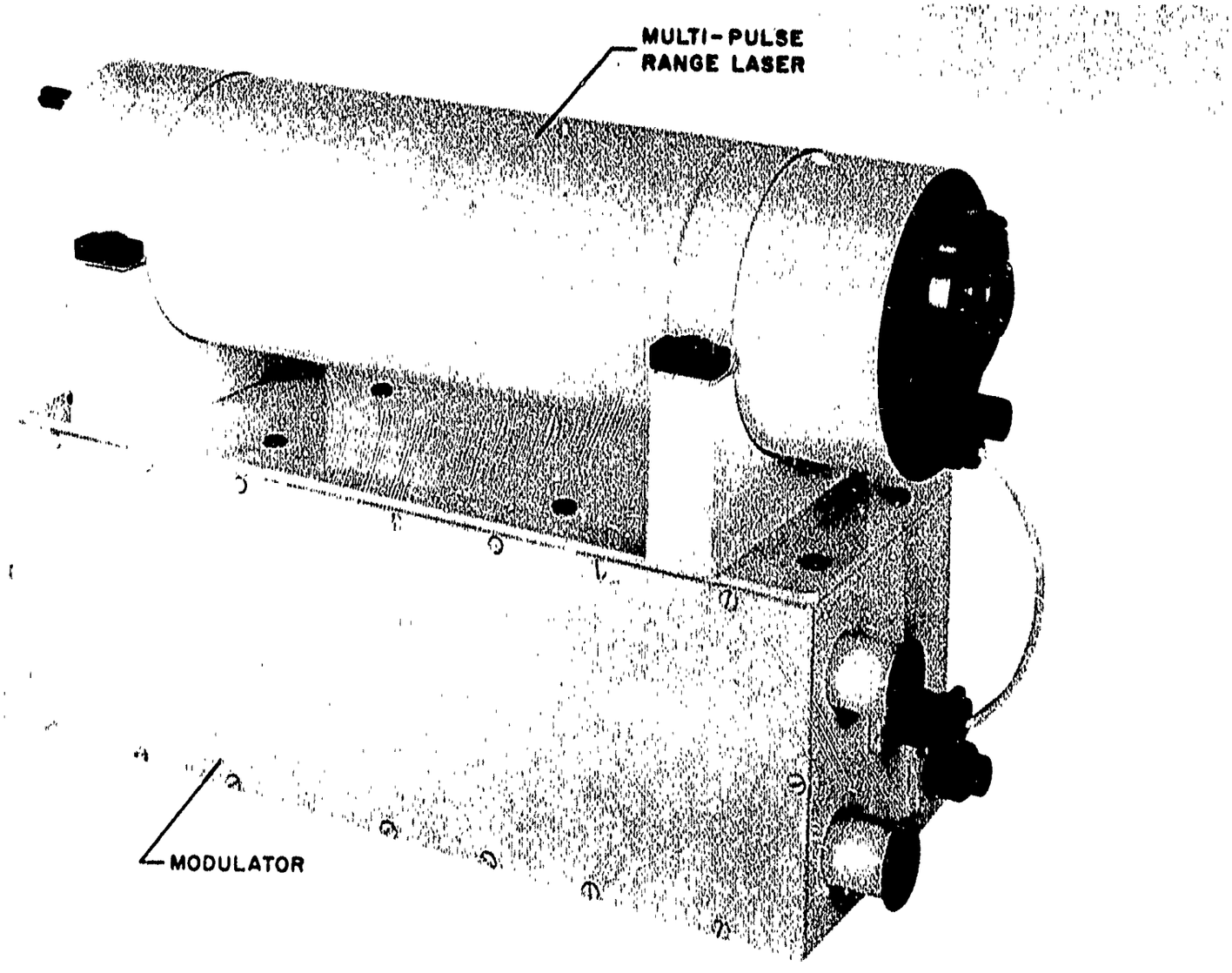

Fig. 5. Experimental multi-pulse laser (EML).

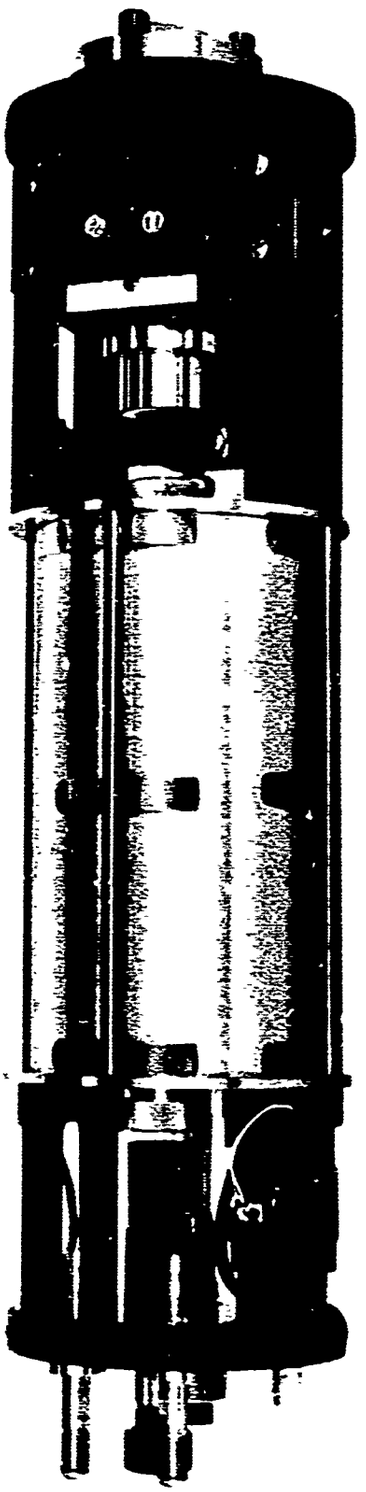

Fig. 6. Internal view of EML (top-quarter view).

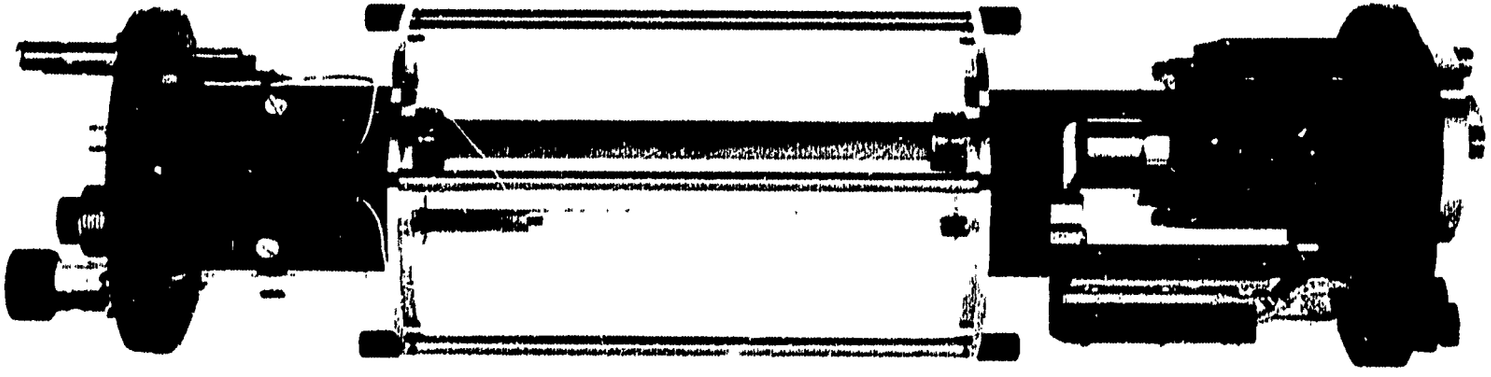

Fig. 7. Internal view of EML (side view, without reflectors).

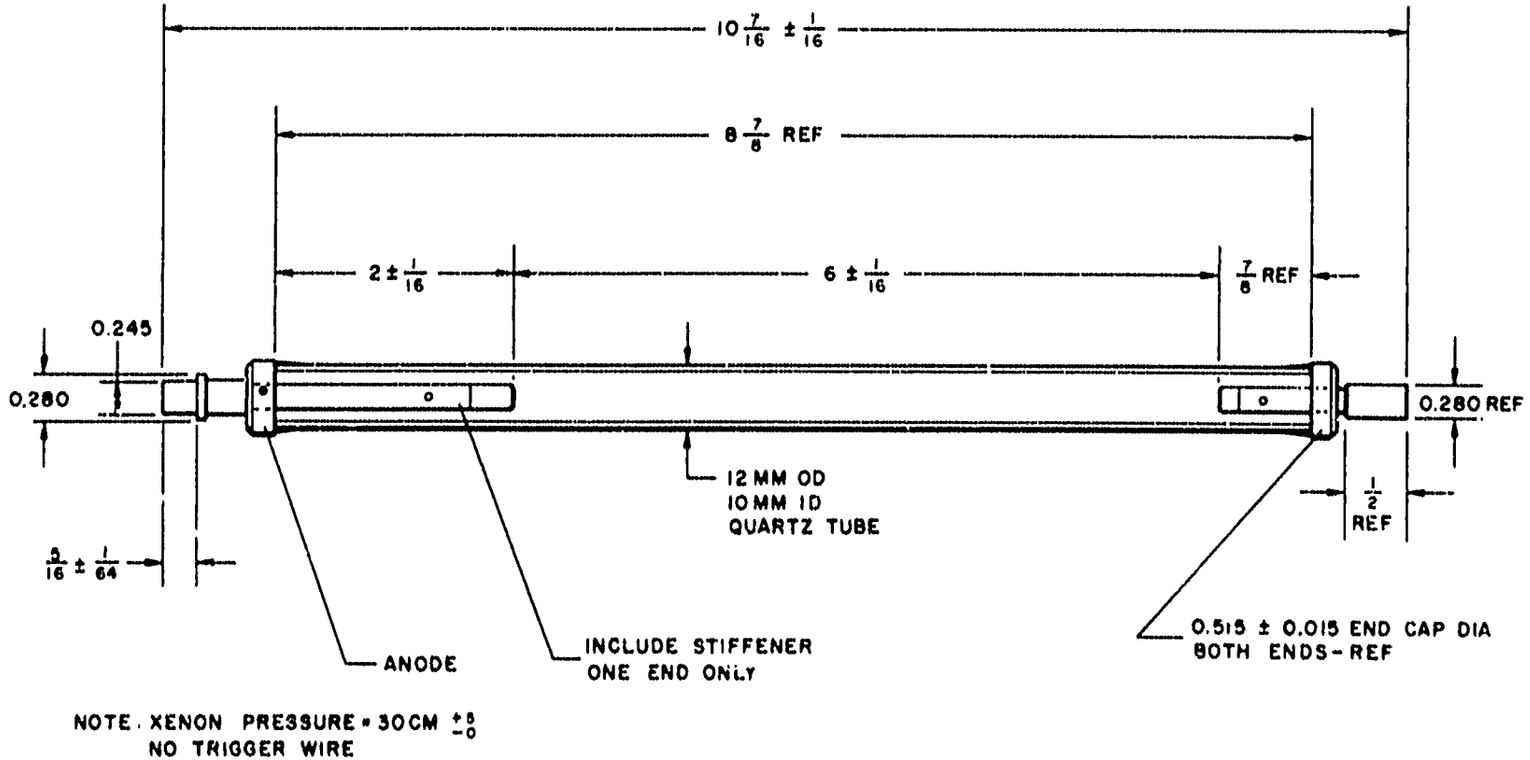

Fig. 8. EML Flashtube, Type FX-81-6B.

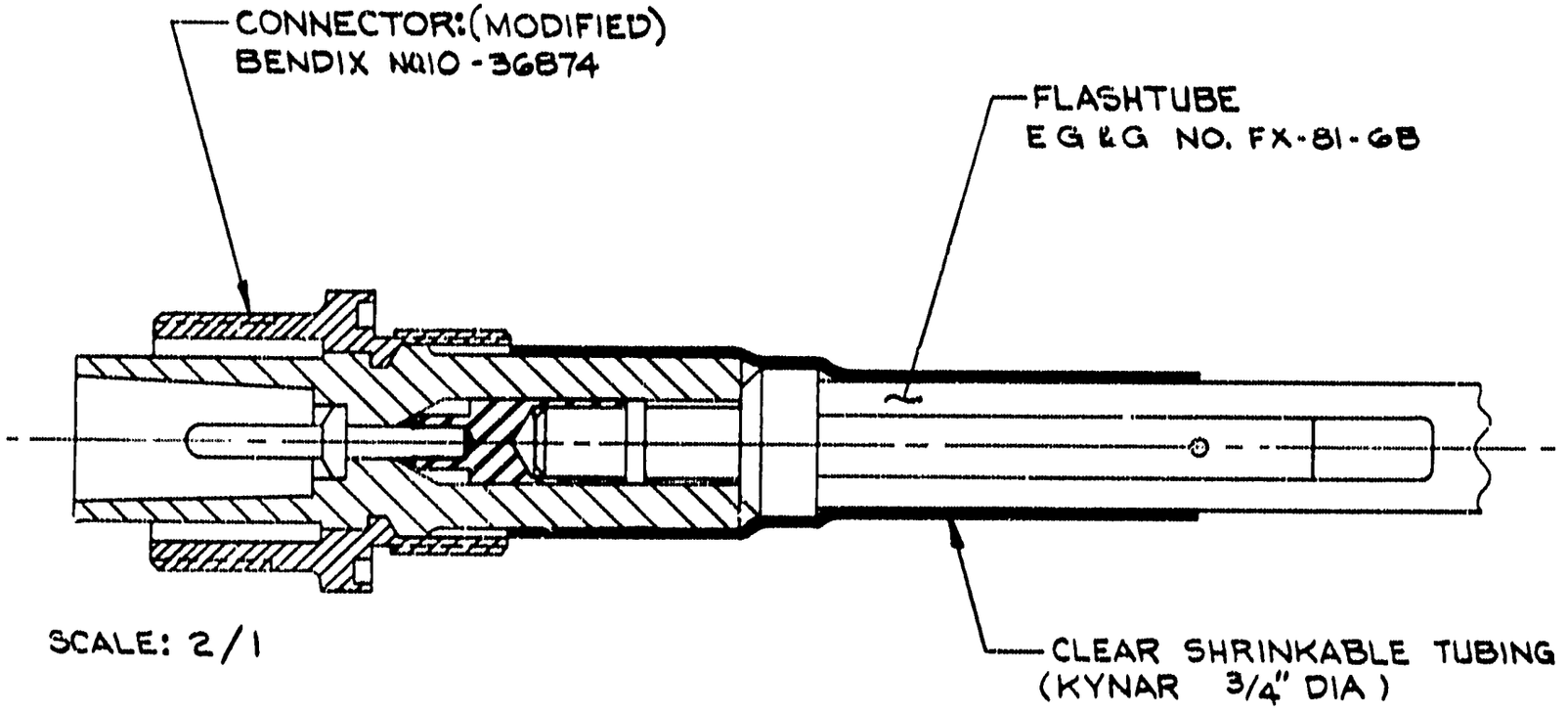

Fig. 9. Flashtube-anode connector assembly.

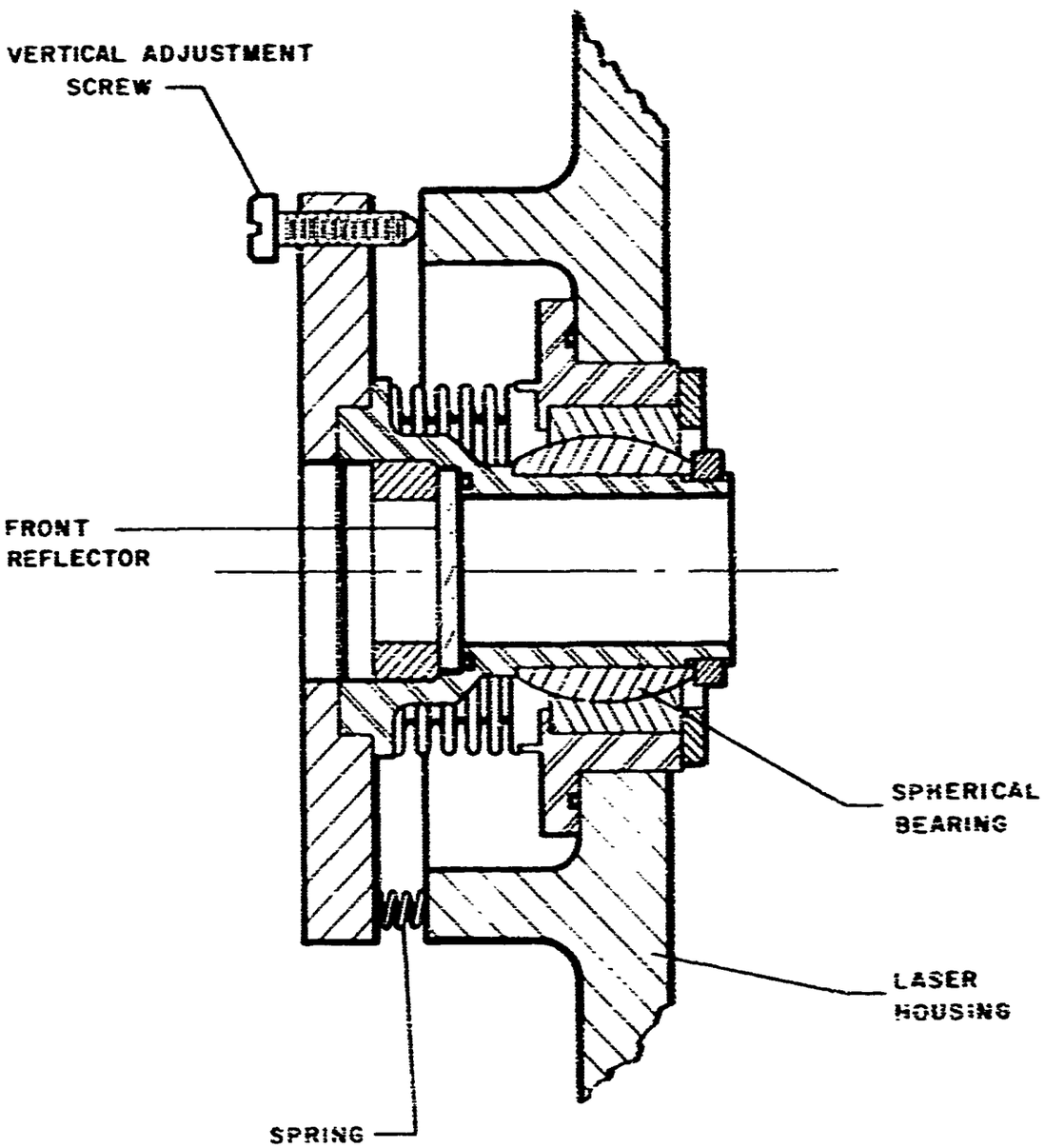

Fig. 10. Spherical bearing mirror mount.

that are perhaps unique. The flashtube-connector assembly is designed for safe operation in excess of 5 kV dc (30 kV peak), and can be conveniently and quickly mounted into the laser without compromising the dust and moisture seal of the housing. The spherical bearing support for the front mirror has three degrees of freedom in rotation, and is virtually incapable of any other motion with the loads that are normally applied. It permits angular adjustment about two orthogonal axes with negligible cross-coupling at small angles, and is rugged, compact, simple, and inexpensive compared to a two-axis gimbal mount.

The Kerr-cell modulator schematic and its physical appearance are shown in Fig. 11. A vacuum-tube modulator is used because it is the only type that operates reliably at the fast switching rates anticipated (up to at least 50 kHz). The principal disadvantage of this type of modulator is its relatively high impedance, of the order of 100 ohms compared to a fraction of an ohm for some thyratron and spark-gap switches. The modulator output waveshape across the Kerr cell, shown in Fig. 12, has a rise time of about 85 nanoseconds. The laser Q-switching time is considerably less than this because of the non-linear relationship between the transmission of a Kerr cell and its operating voltage. The shutter is more than 75% open when the bias voltage has dropped 50%, so that the Q-switching time is believed to be less than 45 nanoseconds.

The programmer used to trigger the EML modulator develops 1 to 5 pulses, as programmed. The output pulses of the programmer are +120 v peak with a rise time of 0.1 microsecond; the delay between the first pulse and the fiducial trigger pulse* can be varied from 50 to over 1000 microseconds, and that between successive pulses can be varied from 7 to over 200 microseconds.

The energy-storage network used with the EML is a lumped transmission line as shown schematically in Fig. 13. The pulse shape across the flashtube is approximately rectangular and is about 460 microseconds in duration. The laser is normally operated at a storage network voltage of 3 kV, or 2200 joules of stored energy; losses due to dissipation in the network inductors, transmission cable, and connector are estimated to be 15%.

---

*Normally, the programmer fiducial trigger also fires the pump flashtube.

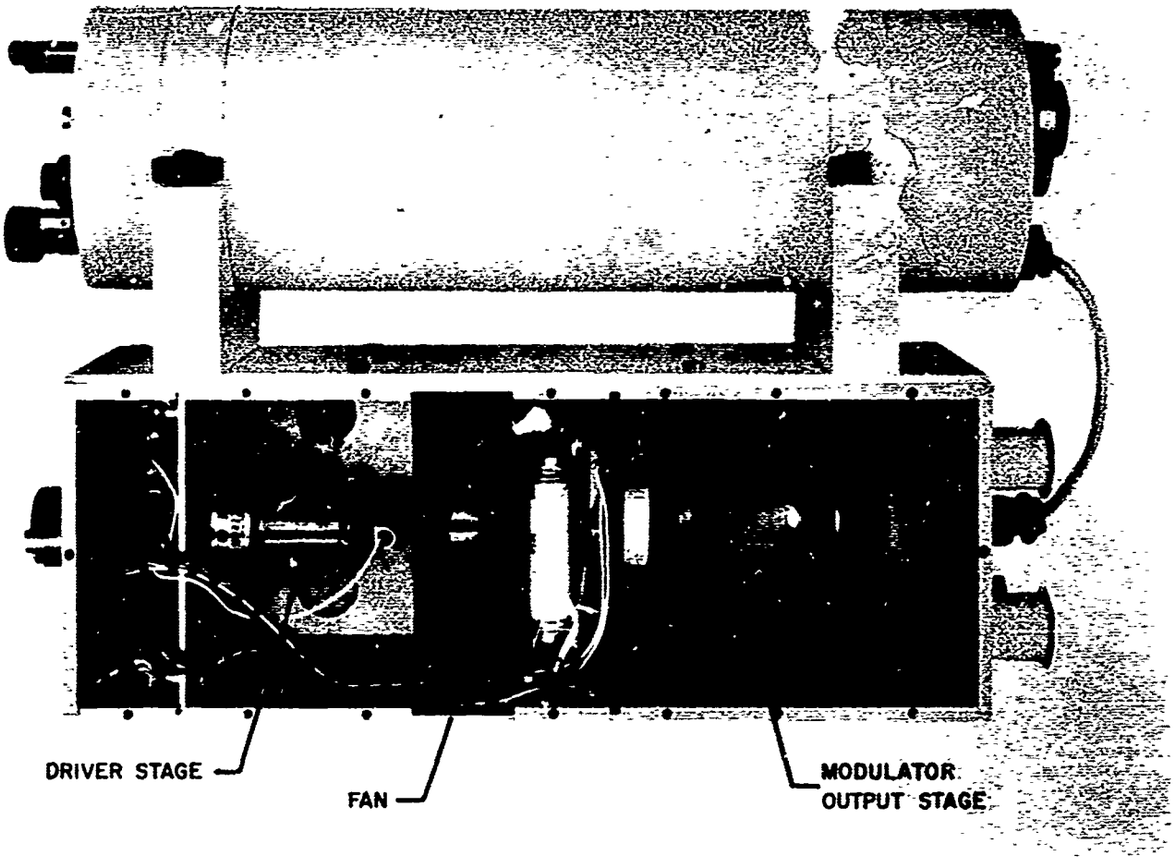

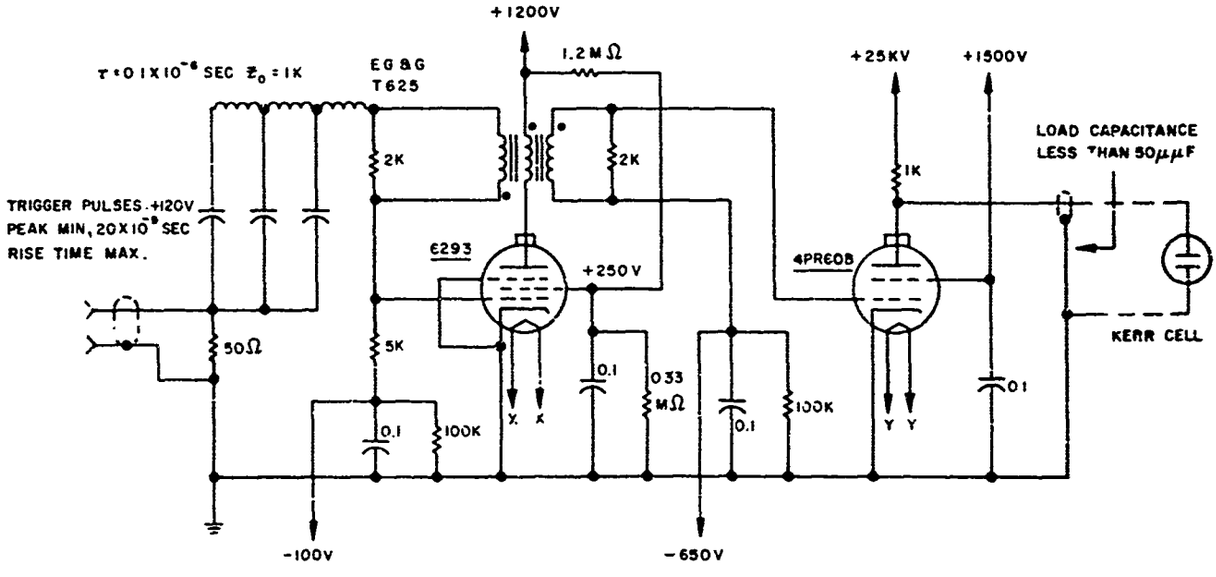

Fig. 11. EML modulator.

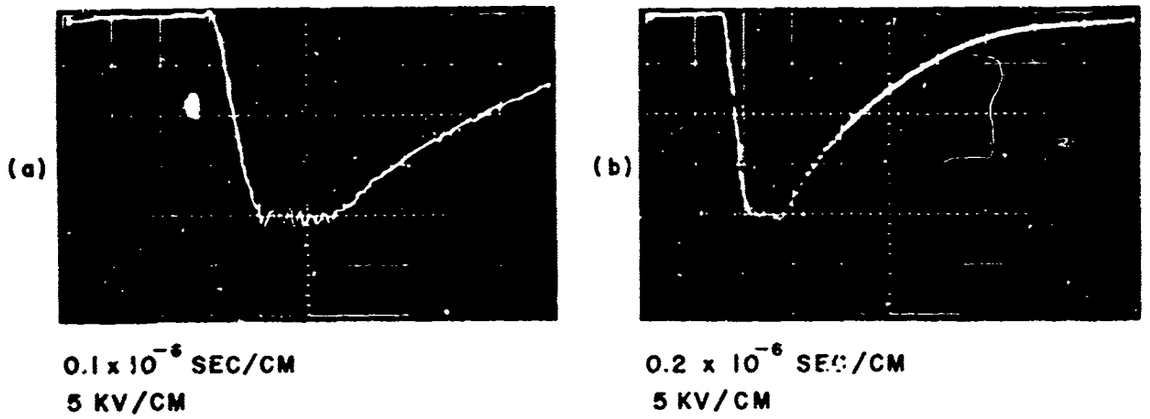

Fig. 12. EML modulator output waveform.

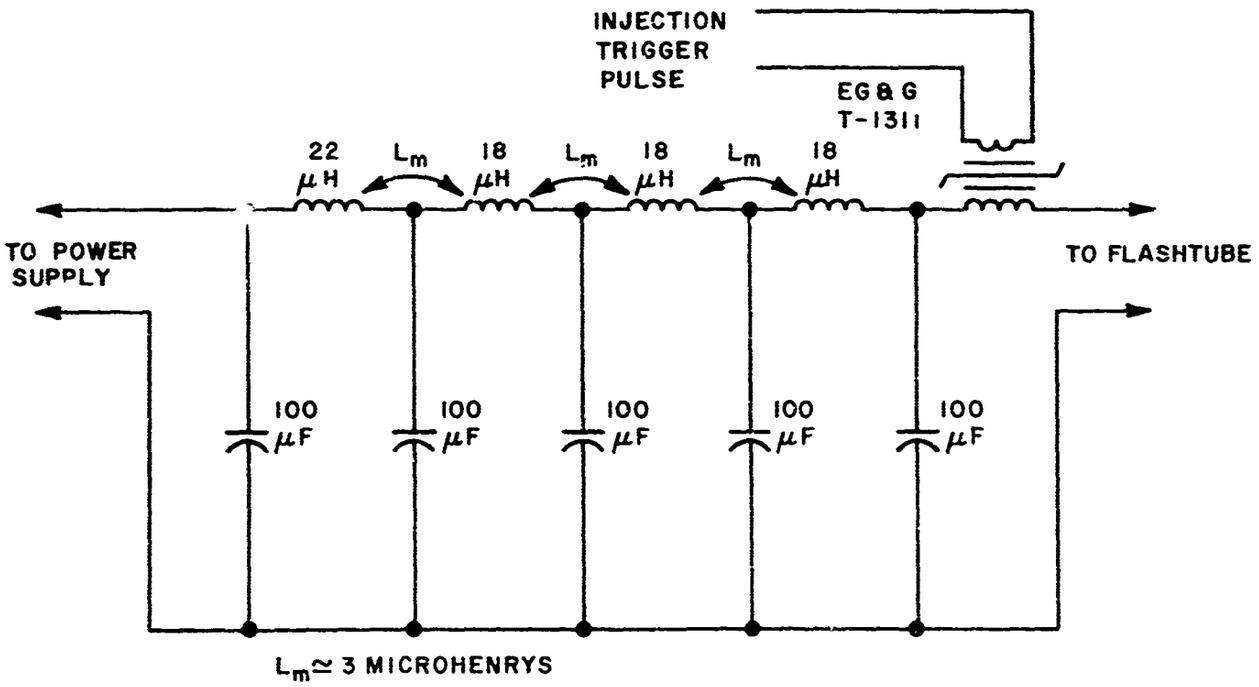

Fig. 13. EML energy-storage network.

3.2 PERFORMANCE CHARACTERISTICS OF THE EML

3.2.1 Normal Mode Energy Output

All the data discussed in this sub-section were taken at a storage network voltage of 3 kV, that is, 2200 joules of stored energy and approximately 1800 joules of flashtube energy. Energy measurements were made at various times with three different instruments: an EG&G Model 580-22 Radiometer,* an EG&G Model 560 "Lite Mike",** and an IT&T Corp. Type F114-A Biplanar Photodiode (S-20 surface) plus integrator.** The measurements made with these instruments agreed within 20%.

The normal-mode output of the EML under a number of different conditions is summarized in Table 3. The results shown are in agreement with more than 90% of many measurements made over a period of several months. These data show that the laser output was increased 33% when a polished-silver reflector surface with a 5-microinch finish was substituted for a specular aluminum surface in the cylindrical pumping configuration used. Polished silver has about a 16% higher reflectance than aluminum*** in the pumping spectrum. The Kerr cell and polarizer caused a 40% drop in normal-mode laser output. The normal-mode efficiency of the laser itself is about 0.6% near room temperature with the Q-switch installed, and is about 1.0% without it. The overall efficiencies (i.e., with respect to the stored energy) are about 0.48% and 0.80% respectively.

Normal-mode lasing generally occurred over a period of about 300 microseconds, or 66% of the pumping period. Figure 14 (a thru e) shows a number of oscillograms of normal-mode energy measurements. In this series, the Kerr-cell bias voltage is increased from 0 to the $\lambda/4$ retardation voltage of 26 kV. Note that the bias has little effect on the output until it is greater than about 10 kV, or almost one-half of the $\lambda/4$ retardation voltage.

---

*Laser beam directly incident on radiometer diffusing aperture.

**Laser beam reflected from diffuse target; see AFCRL Final Report (Contract AF 19(628)-5516), to be published.

***With "Alzak" specular finish. (Note: all results discussed in the remainder of sub-section 3.2 were obtained with silver-plated reflectors.)

(a)

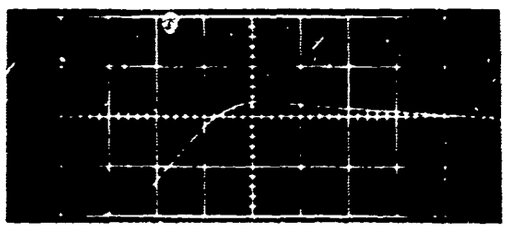

0.1 MSEC/CM
5 V/CM
KERR-CELL BIAS = 0

(d)

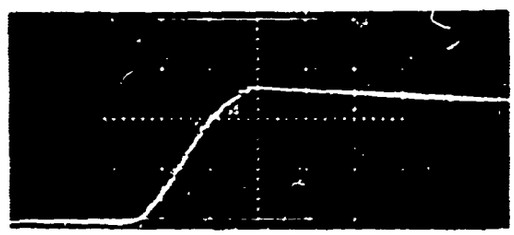

0.1 MSEC/CM
2 V/CM
KERR-CELL BIAS = 20 KV

(b)

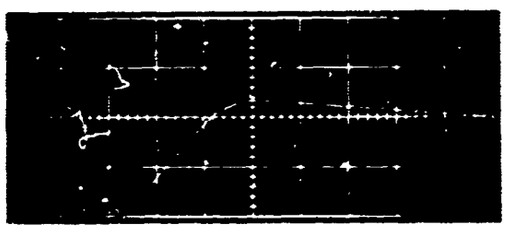

0.1 MSEC/CM
5 V/CM
KERR-CELL BIAS = 3 KV

(e)

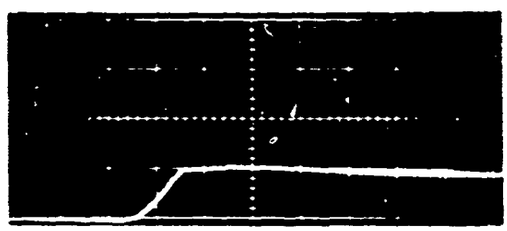

0.1 MSEC/CM
2 V/CM
KERR-CELL BIAS = 26 KV

(c)

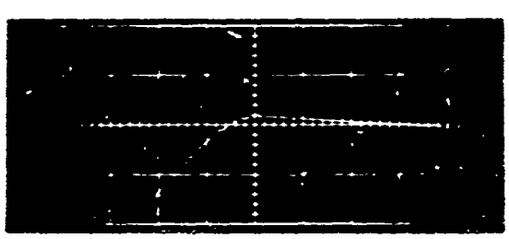

0.1 MSEC/CM
5 V/CM
KERR-CELL BIAS = 10 KV

(f)

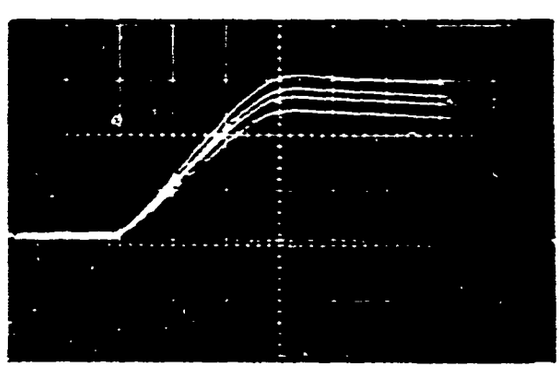

0.1 MSEC/CM
5 V/CM
4 SHOTS, SPACED $4\frac{1}{2}$ SEC APART

STORED ENERGY = 2200 JOULES
VERTICAL CALIBRATION = 0.83 JOULE/V

Fig. 14. Normal-mode energy oscillograms.

Table 3. Normal-mode output of EML.

Conditions	Average Energy Output (joules)	Spread
Specular aluminum reflectors, without Kerr cell or polarizer	13.5	±20%
Specular aluminum reflectors, with Kerr cell and polarizer	8	±10%
Silver-plated reflectors, without Kerr cell and polarizer	18	±20%
Silver-plated reflectors, with Kerr cell and polarizer	10.5	±20%
Stored energy = 2200 joules. Estimated inductor, line, and connector losses ≃ 15%.		

A number of measurements were made to determine how the normal-mode output drops due to the temperature rise caused by a number of shots spaced 4 seconds apart without cooling. The average percentage drop in output (referenced to the output of the first shot) is 8%, 13%, 22%, and 33% for shot numbers 2, 3, 4, and 5, respectively. Figure 14f is an oscillogram of one output vs temperature run. (Similar measurements were made of the giant pulse output energy vs temperature. See paragraph 3.2.2.)

3.2.2 Giant Pulse Energy Output

The output energy of Q-switched pulses was measured in the same manner and with the same equipment as the normal-mode output. Relative values of these measurements are therefore expected to be more accurate than the absolute values of either. Typical giant pulse output energy oscillograms with 1 and 5 giant pulses in a single pumping period are shown in Fig. 15(b) and 15(c); the corresponding normal-mode output is shown in Fig. 15(a).

Table 4 is a summary of measurements made to experimentally determine what part of the normal-mode output is extracted in one or

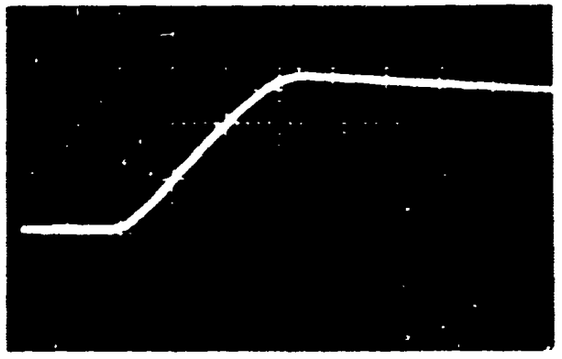

(a)

NORMAL-MODE OUTPUT

0.1 MSEC/CM
5 V/CM

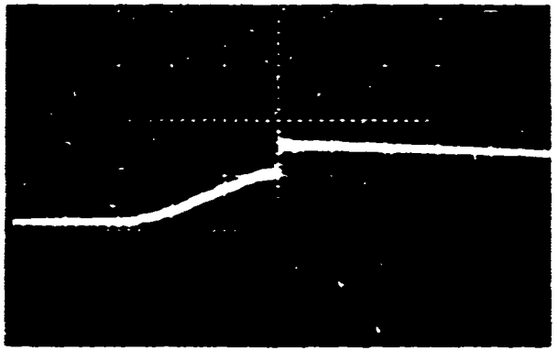

(b)

0.1 MSEC/CM
5 V/CM

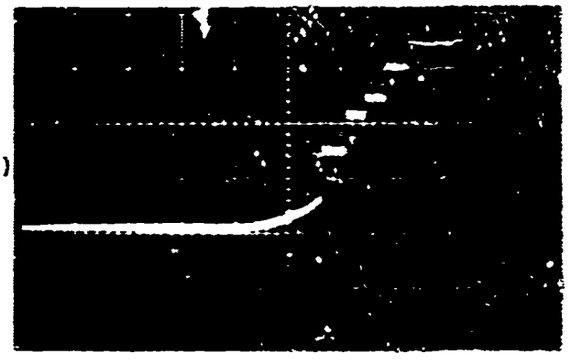

(d)

0.05 MSEC/CM
2 V/CM

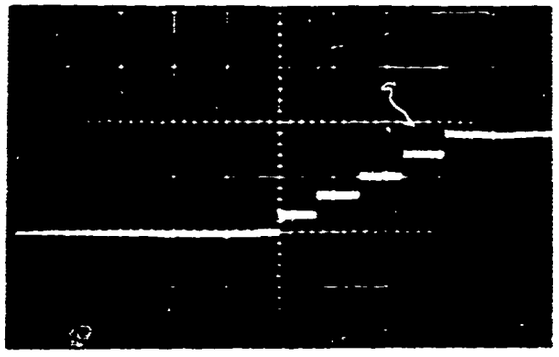

(c)

0.05 MSEC/CM
5 V/CM

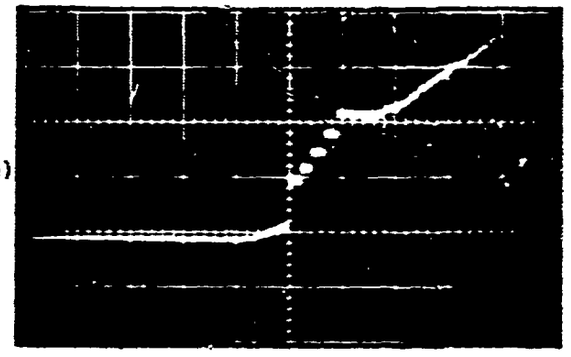

(e)

0.05 MSEC/CM
2 V/CM

STORED ENERGY = 2200 JOULES
VERTICAL CALIBRATION = 0.83 JOULE/VOLT

Fig. 15. Giant pulse energy oscillograms.

Table 4. Multi-pulse energy output of EML.

Period Between Giant Pulses (10^{-6} sec)	Max No. of Pulses	Average Energy/Pulse (joules)	Total Output Energy (joules)	Spread in Energy/Pulse (joules)
-	1	1.7	1.7	1.6 to 1.8
65	4	1.6	6.4	1.5 to 1.7
47	6	1.6	9.6	1.5 to 1.7
40	7	1.5	10.5	1.4 to 1.6
27	10	1.1	11.0	1.0 to 1.3
18	15	0.8	12.0	0.5 to 1.1
9	30	0.4	12.0	0.2 to 0.7

Normal-mode output ≃ 12.0 joules.

Lasing period ≃ 300 microseconds.

Pumping period ≃ 460 microseconds.

Stored energy = 2200 joules.

more giant pulses, and the energy per pulse. The outputs of 1 to 5 giant pulses were measured directly; the values for the total number of pulses and the total energy output are extrapolated when the interval between pulses is less than 60 microseconds. Fig. 15 (d to e) are records of data taken in this run. These data are plotted in Fig. 16 in normalized form. It is significant that the efficiency of the laser increases with the number of giant pulses developed during a pumping period, and particularly that the energy per giant pulse remains almost constant up to about 7 pulses when over 80% of the normal-mode output has been extracted. Although this data was taken with a particular laser, it is believed that the normalized results apply to Q-switched ruby lasers in general when operated at or near room temperature. In a general way these results are physically reasonable. The approach to normal-mode output as the number of pulses becomes large can be expected, since this condition is akin to synchronizing the normal-mode spikes. The spread in the output energy per pulse (Table 4) can also be expected to increase as the interval between pulses decreases, due to the statistical nature of the changes in state involved (sufficient data was not taken to experimentally determine the statistical distribution of the energy per pulse.)

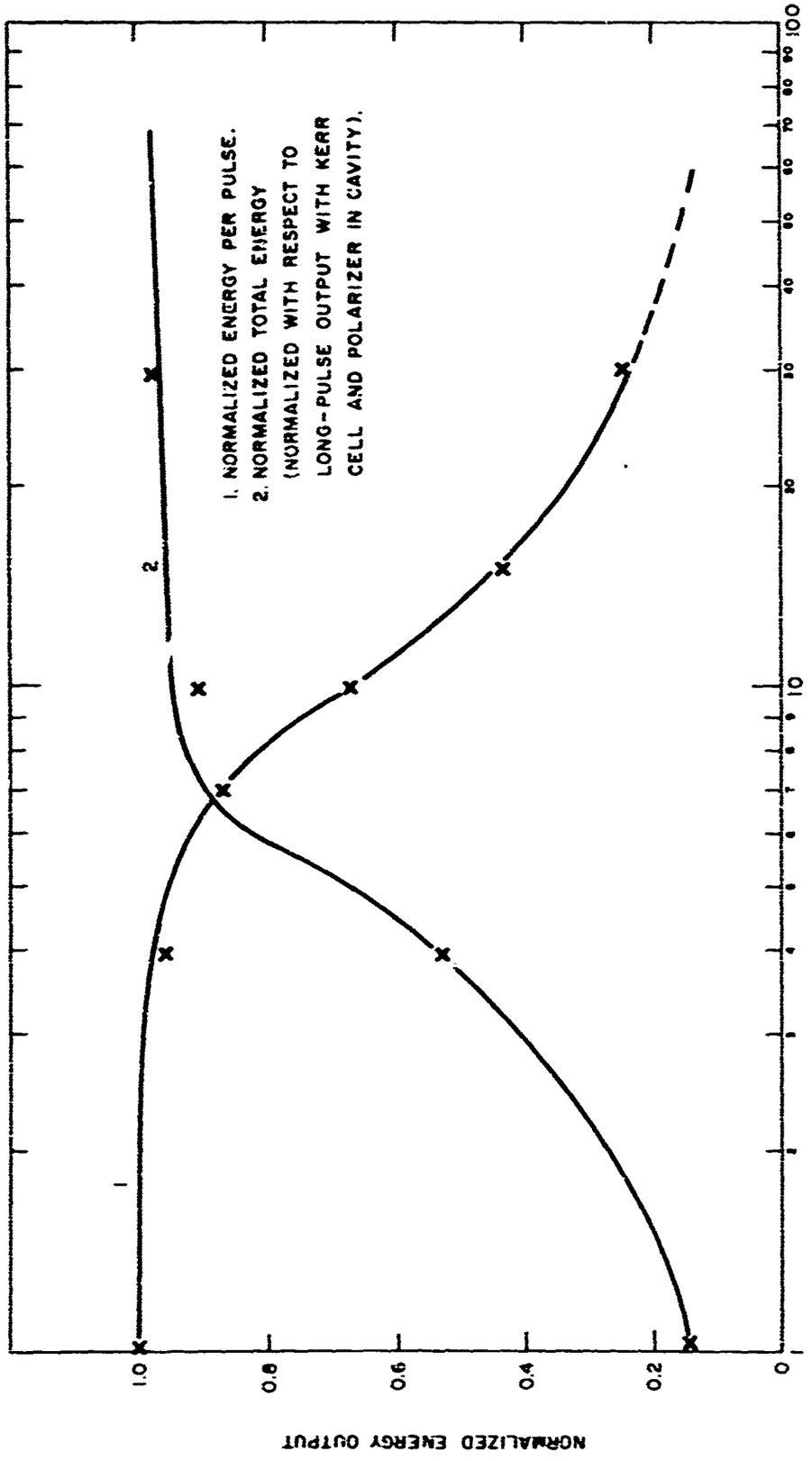

Fig. 16. Normalized EML output characteristics.

Over 80% of the giant pulse energy measurements made during a period of several months are within 1.3 (±20%) joules with 5 or less properly phased pulses generated per pumping period. For reasons that are not clear, this value dropped to 1.0 (±20%) joules toward the end of the experiments.

A number of measurements were made to determine how the giant pulse energy changes with the temperature rise resulting from a number of closely spaced shots. The shots were spaced 4 seconds apart; no cooling was used, and the crystal was initially at a room temperature of about 80°F. After five shots, the energy in a single giant pulse (per pumping period) increased from 10% to 20% of its initial value. Refer to Fig. 17(a). After 5 such shots, the total energy in 5 giant pulses (per pumping period) decreased less than 10%. Refer to Fig. 17(b). This is a considerably smaller drop than the 33% change in the normal-mode output under the same conditions (paragraph 3.2.1). The inverted population losses between pulses and the laser efficiency during a pulse are both functions of the fluorescent efficiency of the crystal. The fluorescent efficiency decreases with rising temperature*, and it is assumed that the resulting drop in population losses compensates, or more than compensates, for the lower laser gain. It can be expected that this stabilizing mechanism will be considerably less effective as the multi-pulse energy output approaches more closely that of the normal mode; insofar as temperature stability is concerned, it may be desirable to keep the multi-pulse output energy to less than 80% of the normal-mode output. Figure 17(c) shows the disproportionate loss of energy in the first and last pulses as the temperature rises and the threshold energy increases; this can be avoided or greatly reduced by proper phasing with respect to the pumping cycle. These measurements indicate that cooling the laser crystal would probably not have a significant effect on giant pulse output energy during a burst of several closely spaced shots, assuming any appreciable cooling could be achieved under such transient conditions.

3.2 3 Giant Pulse Power Output

In the analysis of optical radar using energy detection (Section 2), a fundamental quantity is the received energy within the resolvable time interval, τ. The assumptions concerning τ are that the receiver cannot

*Ackerman, Sumner, "Design Study of Advanced Geodetic Laser System," AFCRL Scientific Report No. 1 (Contract No. AF 19(628)-5516), pp 18 and 21.

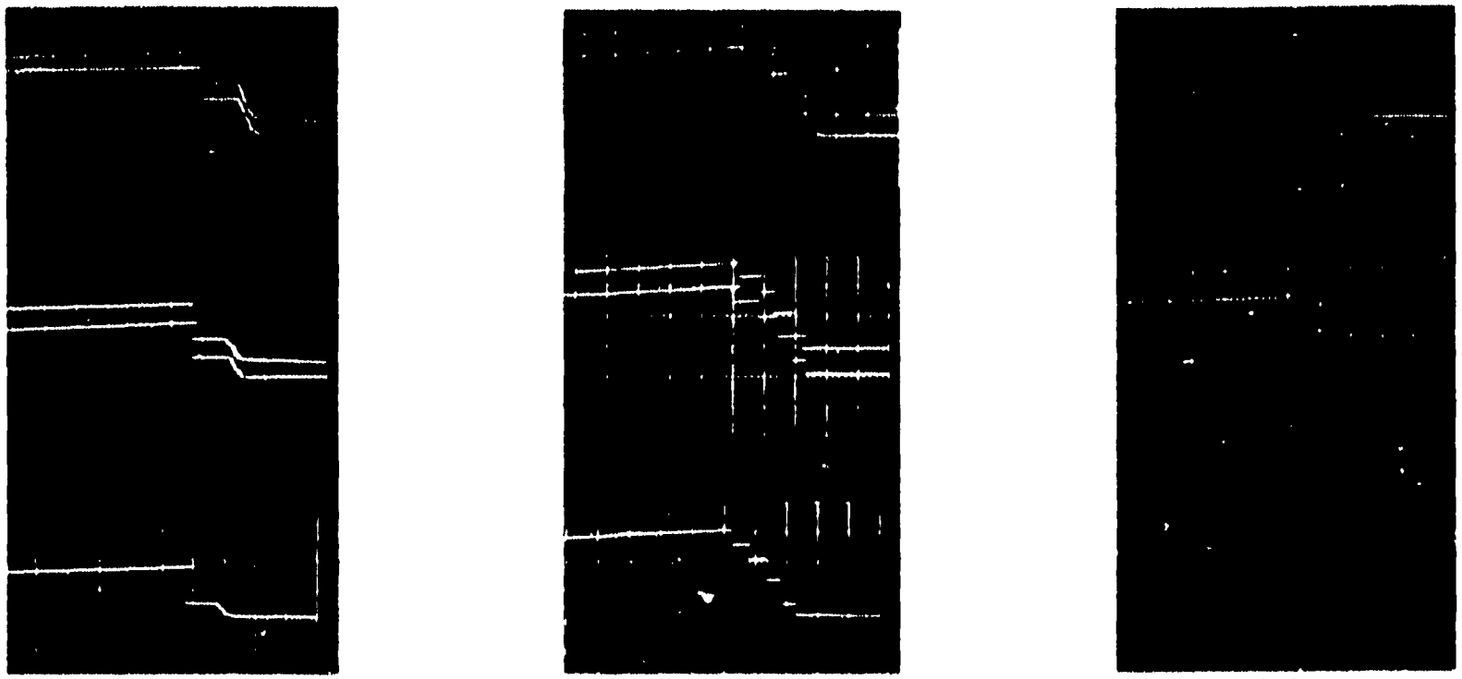

Fig. 17. Giant pulse output energy during burst.

resolve a photoelectron count in a smaller time increment and that only the transmitted energy within this time interval will contribute to the signal.* A practical requirement is that τ is also a satisfactory limit on range resolution. Under these conditions, the distribution of the energy within τ, i.e., power as a function of time, is irrelevant (at least to a first order approximation). In particular, the "peak power" of the pulse can be a misleading criterion; it has meaning only to the extent that the power waveshape is simple, is known, and therefore has an unambiguous relationship with the energy content of the pulse and the pulse duration. It is easy to postulate examples where this may not be the case, and some of these will be shown. A more fundamental and useful quantity for describing the pulse quality for range detection is J_τ, the total energy of the pulse within the time interval τ, where τ may take appropriate values, usually of the order of 10^{-8} seconds; τ will be expressed here in nanoseconds. Additional subscripts can be used to indicate transmitted energy, received energy, etc. Power measurements will be used here largely for evaluating J_τ by integration**; any other use of power, or reference to peak power, is in deference to custom.

About half of the output power measurements were made with an IT&T Corp. Type F114-A Bi-planar Photodiode, using the bias and output circuits recommended by the manufacturer,*** and a Tektronix, Inc., Model 585A Oscilloscope. The total rise time of this combination is 5 nanoseconds. (Other power measurements were made with a Tektronix, Inc., Model 555 Oscilloscope having a rise time of 12.5 nanoseconds, but these data are not used herein.)

Some typical output measurements are shown in Fig. 18. Note that the peak power output of the pulses in Fig. 18(c) and 18(e) is significantly higher than that of the pulses in Fig. 18(a) and 18(b), but the latter have a higher energy, J_{30}. If $\tau = 30 \times 10^{-9}$ seconds, the lower peak power pulses will contribute more to the received signal.

---

*Energy transmitted elsewhere within the observation time T could be interpreted as noise if it is detected.

**A K&E Co. Type 423GM Planimeter was used to integrate power waveforms.

***IT&T Corp. Industrial Laboratories Bulletin FW114-A (10/1/63). Rise time under conditions used is less than 10^{-9} seconds.

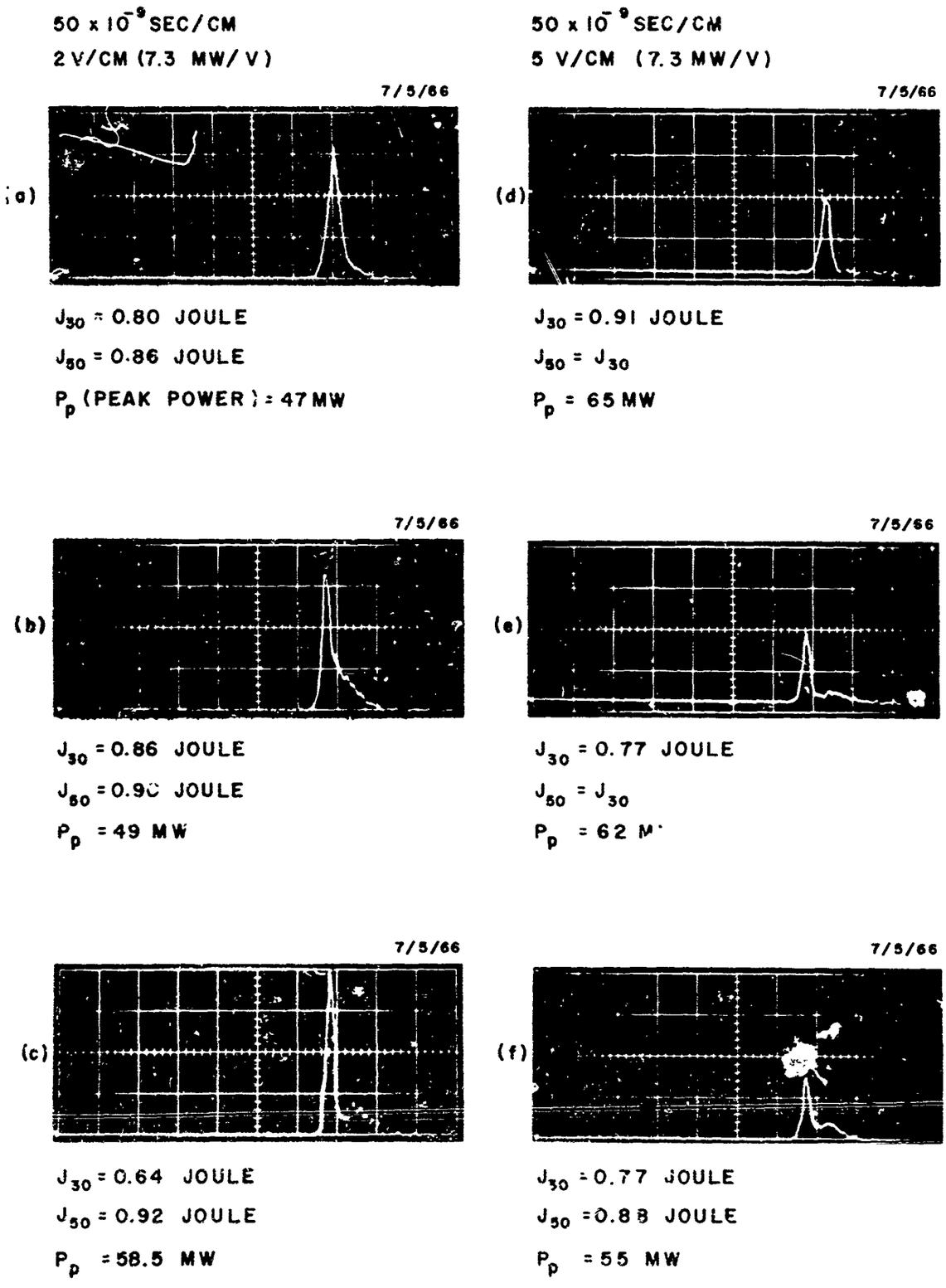

Fig. 18. Ciant pulse power waveforms.

In general, the giant pulses had 0.8 ± 20% joule in a 30 x 10^{-9} second period when measured by integration of the power output waveform and had 1.1 ± 20% joules by direct integration of the photodetector output. The difference may be caused by a number of things, including measurement errors, distortion of power waveshape with respect to that normally expected, and after-pulsing which does not show on the pulse power records. The effect of distortion is shown particularly in Fig. 18(c), 18(e), and 18(f), and shows to a lesser extent in Fig. 18(b). The small, high-frequency modulation that appears on these oscillograms is believed due to electrical noise pickup and/or line reflections. The gross shapes of the curves are believed to accurately show the giant-pulse behavior of the laser within the time resolution of the measuring equipment. This distortion is probably due to the relatively slow Q-switching time of 45 nanoseconds. Judging from the marginal performance now experienced, if this time is reduced to less than 30 nanoseconds*, the giant pulse power output is expected to be more consistent and symmetrical and to almost always contain over 80% of the pulse energy within a period of 30 nanoseconds.

Perhaps the best way to measure and monitor the giant pulse output is by electronic integration of the photodetector output, using an integration circuit capable of reproducing the fast output step function without serious distortion. If a 93-ohm coaxial line is used for signal transmission, the integrating capacitor at the detector can be about 0.005 μF. An output voltage of the order of 10^{-1} to 1 volt will be obtained if the permissible detector peak current is approximately 10^{-1} ampere. The detector and oscilloscope rise time should be less than 5 nanoseconds; if the rise time is much more than this, the circuit may be used to monitor the relative performance of the laser.

The oscilloscope was triggered externally by the input trigger pulses to the modulator when taking the oscillograms shown in Fig. 18. The total delay between the trigger and giant pulses averaged close to 350 nanoseconds and the time jitter is within ± 15 nanoseconds, even though no special effort was made to minimize timing uncertainty. Jitter should be reduced to less than ± 10 nanoseconds when the rise time of the modulator input trigger is reduced, the modulator itself is carefully designed toward this end, and the Q-switching time is reduced to about half its present magnitude.

---

*By using a lower-capacitance, lower-operating-voltage Pockels cell.

3.2.4 Beam Divergence

Three different crystals were used with the EML. The beam divergence of only one of these was measured; this crystal has a rough-ground body surface, is of standard grade, and is probably the poorest of the crystals, optically.

The far-field beam of this crystal is roughly elliptical, with a total divergence at half-intensity points of about 10 milliradians by 14 milliradians. The beam spread was measured by two methods; the beam reflection from a distant, diffuse target was photographed, * and a series of energy measurements were made with successively smaller aperture masks covering the beam reflection. The results obtained by the different techniques agreed reasonably well.

It is expected that the total beam divergence obtained with crystals of superior quality will be less than 10 milliradians, as is generally reported for laser configurations similar to that of the EML. Relatively little attention was given to the beam characteristics of the EML quantitatively because of the expectation that the multi-pulse laser is not peculiarly different in this regard to conventional single-pulsed Q-switched lasers.

3.3 NOISE MEASUREMENT

The noise energy, $\bar{N}_n$, has been defined as the average number of photoelectrons emitted by the detector photocathode in an interval of time τ. $\bar{N}_n$ is easily measured through its relationship to the average (i.e., d-c) anode current of the photodetector. The number of photoelectrons emitted by a photocathode is equal to

$$\frac{1}{e}\int_0^t i\,dt$$

*AFCRL 65-671, pp. 52-60.

where e is the charge on the electron (1.592×10^{-19} coulombs) and i is the photocathode current in amperes. Therefore,

$$\bar{N}_n = \left[\frac{10^{19}\,\tau}{1.592\,G}\right] \bar{i}_a, \text{ photoelectrons} \tag{15}$$

G is the current gain of the (photomultiplier) detector and $\bar{i}_a$ is its average anode current.

Figure 19 shows oscillograms of photomultiplier outputs at different average anode currents due to a range of low to high background illumination levels. The current gain is about 10^7, so that for $\tau = 30 \times 10^{-9}$ seconds,

$$\bar{N}_n = 18.8 \times 10^3\ \bar{i}_a \text{ photoelectrons} \tag{16}$$

Most photomultipliers cannot develop an average anode current much higher than 10^{-3} ampere without becoming fatigued or permanently damaged. For this reason alone, a value of $\bar{N}_n$ much greater than 20 cannot generally be tolerated. Under usual nighttime conditions, $\bar{i}_a$ will be of the order of 10^{-6} ampere, so that $\bar{N}_n$ will be of the order of 10^{-2}. Note that, because of the Poisson distribution of photoelectron emission, the average number of noise pulses over a period T is closely equal to $\bar{N}_n (T/\tau)$, when $\bar{N}_n << 1$.

Background noise can be predicted, of course, if the spectral radiance of the background is known. Spectral radiance, N_λ, is usually expressed in units of watts/m^2/ster/Å, so that the incident power on the detector is

$$P_w = N_\lambda A_R \Omega_R \Delta\lambda\, \epsilon_r \text{ watts} \tag{17}$$

where

A_R = receiver aperture (m^2)

Ω_R = receiver field (steradians)

$\Delta\lambda$ = receiver optical bandwidth (Å)

ϵ_r = optical efficiency of receiver

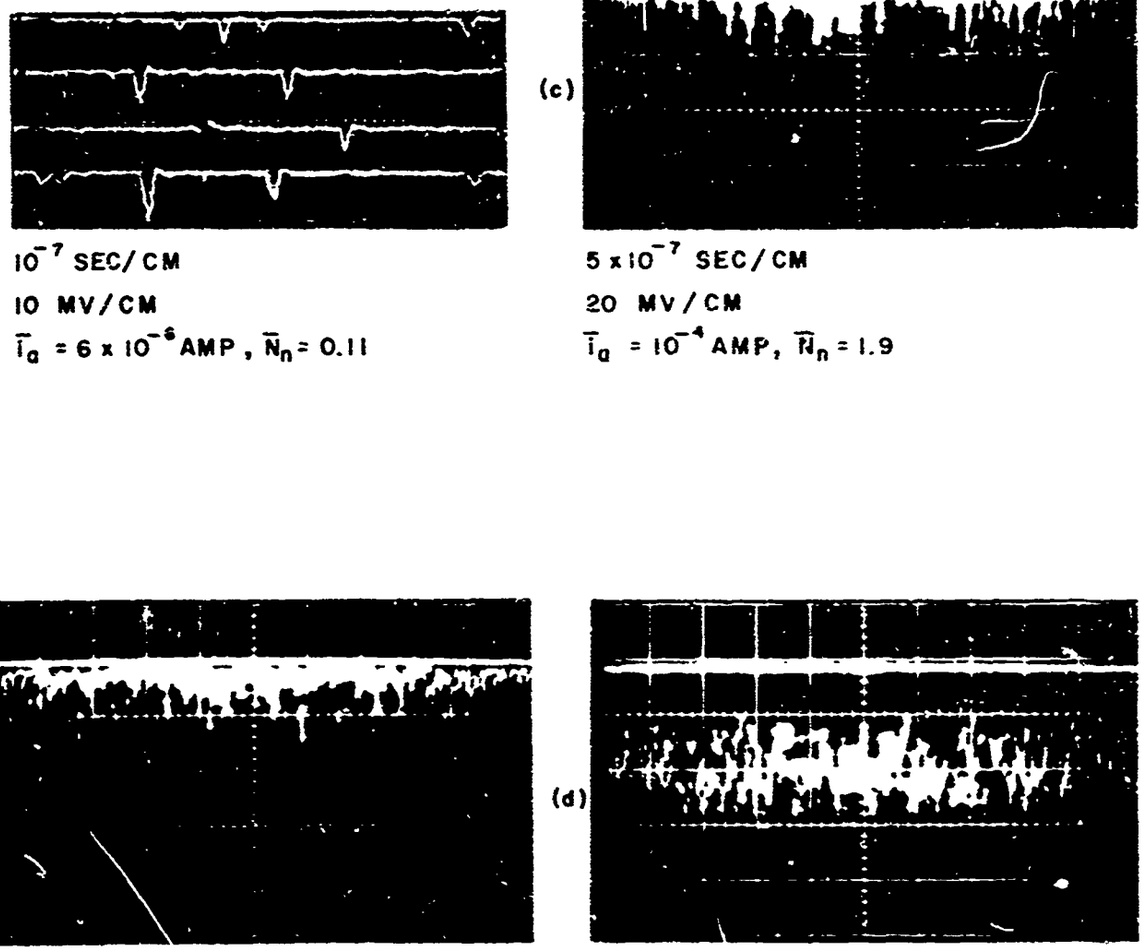

Fig. 19. Photoelectric Receiver noise with various background illuminations.

Then,

$$P_p = P_w \frac{10^{19}}{2.87} \text{ photons/sec at 6943 Å} \tag{18}$$

$$\bar{N}_n = \eta P_p \tau \text{ electrons} \tag{19}$$

where η is the quantum efficiency of the detector(at 6943 Å in this case).

Combining Equations 17-19, and expressing all the quantities in the units customarily used,

$$\bar{N}_n = \eta N_\lambda A_R \left(\frac{\pi}{4} \theta_r^2\right) \Delta\lambda \epsilon_r \tau \left(\frac{10^{19}}{2.87}\right) \text{ electrons} \tag{20}$$

θ_r is the total receiver field in radians.

Representative parameter values for a typical geodetic satellite ranging system are*

$\eta = 0.03$ (S-20 surface at 6943 Å)
$A_R = 2 \times 10^{-2}$ meter
$\theta_r = 10^{-2}$ radian
$\Delta_\lambda = 15$ Å
$\epsilon_r = 0.3$
$\tau = 30 \times 10^{-9}$ second

A relatively high value of N_λ for nighttime conditions is 10^{-5} watt/m^2/ster/Å.** Using these values,

$$\bar{N}_n \simeq 0.073 \text{ electrons (in interval } \tau)$$

*AFCRL Scientific Report No. 1 (to be published), paragraph 1.3. (Contract No. AF 19(628)-5516).

**AFCRL-65-671, pp. 119-124.

SECTION 4

CONCLUSIONS

The technique of programmed multi-pulse range measurement has significant advantages over the single-pulse method, particularly at large range distances and when the target is optically "rough"; such conditions are generally prevelant when measuring the range of satellites from terrestrial stations.

These advantages are due partly to increased transmitter efficiency (in the case of Q-switched ruby lasers), and partly to a reduction in the peak power required per pulse, but most generally and importantly to the statistics of detection in the presence of severe signal scintillation due to the target. The multi-pulse system can have a power gain of from 10 dB to over 25 dB with respect to a single-pulse range finder under such conditions and when the probability of detection is reasonably high, i.e., approximately 97% or better.

When the target is specular, or is well resolved by the receiver, the multi-pulse range finder has a power advantage slightly smaller than the output energy gain due to this mode of operating the laser. For a ruby laser, operating at or near room temperature, the useful energy gain due to multi-pulsing is approximately 8 dB.

In some cases, the multi-pulse range finder may be the only type of pulsed optical radar that is practical, such as when the peak power required of a single-pulse device would cause immediate damage to the laser.

SECTION 5

RECOMMENDATIONS FOR FUTURE WORK

The following programs are recommended as a course of future work:

a. Fabrication and evaluation of a multi-pulse range-finder system as described in this report and in AFCRL Scientific Report No. 1, Contract No. AF 19(628)-5516.

b. Experimental verification of the range detection theory discussed in this report.

NOTE

The aforementioned experiments could be conducted on the basis of the relative statistical performance between single- and multi-pulse range detection, so that the magnitudes of numerous parameters that would be difficult to evaluate accurately need not be known.* A long-distance terrestrial range such as that between AFCRL, Bedford, Mass. and Mt. Wachusett, Princeton, Mass. may be used. A single cube corner and an assembly of them would constitute a specular and optically "rough" target respectively. The EML, with necessary programming accessories, would be ideal for these experiments, single and multi-pulse data is, of course, obtained simultaneously. Perhaps the most difficult aspect of such experiments will be the elimination of significant scintillation due to the atmosphere, particularly over a terrestrial range that is well populated and industrialized, as is the one suggested. A different location would be preferable, but there is a fair likelihood that reasonably stable atmospheric conditions will be experienced at times over this range.

*For example, atmospheric transmission, the beam spread, and other deterministic characteristics of the reflectors, and the transmitter energy output from shot to shot.

c. A theoretical study of scintillation phenomena due to the atmosphere and the target, toward a unified model of range detection when both these effects are present. Atmospheric conditions which contribute to signal scintillation should be characterized, just as the conditions for scintillation due to the target have been.

d. Computation of multi-pulse detection in the presence of target scintillation for a wider range of the parameters m, M, $P(D_r)$, and $\bar{N}_S$ (paragraph 2.3). This work is done on a high-speed electronic computer; programs are available for a wide range of cases.

e. Study of alternate methods of processing multi-pulse range finder data in addition to the oscilloscope presentation described herein. The end product of this study would be detailed descriptions of one or more techniques for automatic range measurement and display using multi-pulse data, and the relative performance and cost expectations for each approach. Part of this study can be devoted to visual aids or automatic methods for determining the range from the visual oscilloscope range display.

APPENDIX A

MULTI-PULSE RANGE FINDER DETECTION IN THE PRESENCE OF TARGET SCINTILLATION

A.1 SINGLE-PULSE DETECTION*

If the exact energy of a return can be calculated, at least in principle, the signal photoelectron statistics can reasonably be taken to be Poisson. That is, in the time interval τ, given that the received energy is J_S, the probability that X signal photoelectrons are emitted is given by

$$P(X|J_s) = \frac{(\bar{N}_s)^X}{X!} e^{-\bar{N}_S} \qquad (A1)$$

where $\bar{N}_S$ is the average number of photoelectrons emitted during the signal interval τ, and $\bar{N}_S = J_S \eta$; $\eta \equiv$ detector quantum efficiency.

However, if the signal energy is known only statistically, the resulting photoelectron statistics must be found from an ensemble average of Equation A1. The probability that X signal photoelectrons are emitted is then given by

$$P(X) = \int_0^\infty P(X|J_s)\, p(J_s)\, d J_s \qquad (A2)$$

where $p(J_S)$ is the probability density function of the total energy incident during the pulse. For a deterministically polarized return, the signal photoelectron statistics are found to be negative binomial. That is, the probability that X signal photoelectrons are emitted is given by

$$P_s(X) = \frac{\Gamma(X+m)}{\Gamma(X+1)\,\Gamma(m)} \left[1 + \frac{m}{\bar{N}_s}\right]^{-X} \left[1 + \frac{\bar{N}_s}{m}\right]^{-m} \qquad (A3)$$

*Op cit, p 2.

where m is the number of spacial correlation cells of energy density intercepted by the receiving aperture. When m = 1, that is, when a single cell is observed, the negative-binomial distribution reduces to a Bose-Einstein distribution (geometric distribution),

$$P_s(X) = \frac{1}{1 + \bar{N}_s} \left(\frac{\bar{N}_s}{1 + \bar{N}_s} \right)^X \tag{A4}$$

The noise photoelectrons are taken to have a Poisson distribution. During the time interval τ in which both signal and noise photoelectrons occur, the probability distribution of the total number of photoelectrons is given by

$$P_{s+n}(X) = \left(\frac{m}{m + \bar{N}_s} \right)^m \frac{\exp(-\bar{N}_n)}{(m-1)!} \sum_{j=0}^{X} \frac{(X + m - j - 1)!}{j!\,(X - j)!} \left(\bar{N}_n \right)^j \left(\frac{\bar{N}_s}{m + \bar{N}_s} \right)^{X-j} \tag{A5}$$

where $\bar{N}_n$ is the average number of noise photoelectrons emitted during the time τ.

Performance curves are shown in the referenced work* for the single-pulse case. In the limit of $m = \infty$, the target is specular, and the signal photoelectrons have a Poisson distribution. When the expression for m is evaluated** for geodetic satellite ranging conditions, m = 1.

The notation herein differs from that used by Goodman as follows:

$X \longrightarrow k$
$m \longrightarrow M$
$J_s \longrightarrow W$

*Op cit, p. 2
**Paragraph 2.3

A.2 MULTI-PULSE DETECTION

Detection in the multi-pulse case is determined by the statistical properties of the sum of M independent random variables, where M is the number of pulses per ranging event. For each time interval τ in the total range observation period T, the sum of the M random variables, each representing the number of photoelectrons emitted, is determined.

Since the noise is taken as Poisson distributed, the probability distribution of the sum of M random variables representing the noise is also Poisson distributed, so that,

$$P(X) = \frac{(M\bar{N}_n)^X}{X!} \exp(-M\bar{N}_n) \qquad (A6)$$

For m = 1, and neglecting $\bar{N}_n$ in comparison to $\bar{N}_S$, Equation A4 describes the distribution of signal photoelectrons for a single pulse. The generating function for this distribution is given by*

$$F_X(z) = \frac{p}{1 - qz}, \qquad (p + q = 1) \qquad (A7)$$

where

$$p = \frac{1}{1 + \bar{N}_s}$$

$$q = \frac{\bar{N}_s}{1 + \bar{N}_s}$$

In multi-pulse detection we require the probability distribution of the sum of M random variables, and therefore the generating function of the sum is obtained by multiplying the generating functions for each random variable. Thus, the generating function of the sum is given by

$$F_X(Mz) = \left(\frac{p}{1 - qz}\right)^M \qquad (A8)$$

---

*Feller, W., An Introduction to Probability Theory and Its Applications, Vol. I, John Wiley & Sons, Inc. New York, N.Y., 1957 (2nd Edition), p. 252.

This expression has the same form as the generating function for the negative binomial distribution.* Thus the probability that X signal photoelectrons are emitted is given by*

$$f(X;\, M,\, p) = \binom{-M}{X} p^{M} (-q)^{X} \tag{A9}$$

$$\binom{-M}{X} = \frac{(-M)(-M-1)\cdots(-M-X+1)}{X!}$$

$$\binom{-M}{O} = 1, \text{ by definition.}$$

To use the notation established in the preceding reference, one notes that Equation A3 is of the same form as Equation A9 with the following correspondences:

$$M \longrightarrow m$$

$$p \longrightarrow \frac{m}{m + \bar{N}_s} \equiv p_o \tag{A10}$$

$$q \longrightarrow \frac{\bar{N}_s}{m + \bar{N}_s} \equiv q_o \tag{A11}$$

$$\binom{-M}{X} (-1)^{X} \longrightarrow \frac{\Gamma(X+m)}{\Gamma(X+1)\,\Gamma(m)}$$

For m correlation cells, and still neglecting $\bar{N}_n$ in comparison to $\bar{N}_S$, the probability that X signal electrons are emitted for a single pulse is given by Equation A3. This equation can be equivalently written as

$$P_s(X) \equiv f(X;\, m,\, p_o) = \binom{-m}{X} (p_o)^{m} (-q_o)^{X} \tag{A12}$$

where p_o and q_o are given by Equation A10 and A11

*Op cit, p. 51, (See page 353.)

The generating function for this probability distribution is of the form similar to Equation A8, that is,

$$F_X'(z) = \left(\frac{p_o}{1 - q_o z} \right)^m \tag{A13}$$

For multi-pulse detection, the generating function for the probability distribution of the sum of M random variables is thus given by

$$F_X''(z) = \left(\frac{p_o}{1 - q_o z} \right)^{Mm} \tag{A14}$$

Therefore, the probability that X signal photoelectrons are emitted is given by

$$f'(X; M, m, p_o) = \binom{-Mm}{X} (p_o)^{Mm} (-q_o)^X \tag{A15}$$

A.3 NUMERICAL EXAMPLE

In this example, m = 1, and the average noise energy is sufficiently small so that it may be neglected by comparison with the average signal energy.

Let $\bar{N}_n = 0.01$, M = 1 and 7, and the desired false-alarm* and detection probabilities be 5×10^{-5} and 0.9990, respectively.

A.3.1 Single Pulse (M = 1)

The probability of false-alarm in each τ interval, P (fa), is computed from Equation A6,

$$P(fa) = \sum_{X=S}^{\infty} \frac{(\bar{N}_n)^X}{X!} \exp\left[-\bar{N}_n\right]$$

From Poisson distribution tables,**

$P(fa) \simeq 5 \times 10^{-5}$, when S = 2

*for each of T/τ intervals.

**General Electric Co., op cit, p. 9.

The probability of detection, P (D), is computed from Equation A4,

$$P(D) = \sum_{X=3}^{\infty} P_s(X)$$

It is easier to solve for the probability of no detection, P ($\bar{D}$), where

$$P(\bar{D}) = 1 - P(D) = 0.001 = \sum_{X=0}^{1} P_s(X)$$

Therefore,

$$0.001 = \frac{1}{1+\bar{N}_s} + \frac{1}{1+\bar{N}_s} \cdot \frac{\bar{N}_s}{1+\bar{N}_s}$$

and

$$\boxed{\bar{N}_s = 1999}$$

A.3.2 Multi-Pulse (M = 7)

$$P(fa) = \sum_{X=S}^{\infty} \frac{\left[(7)(0.01)\right]^X}{X!} \exp(-0.07)$$

From the referenced Poisson distribution tables,

$$P(fa) \simeq 5 \times 10^{-5}, \text{ when } S = 3$$

From Equation A9, the probability of no detection is

$$P(\bar{D}) = \sum_{X=0}^{2} f(X; M, p)$$

that is,

$$0.001 = \binom{-7}{0} p^7 + \binom{-7}{1} p^7 (-q) + \binom{-7}{2} (-q)^2 p^7$$

$$0.001 = p^7 + 7 p^7 q + 28 p^7 q^2$$

$$0.001 = \frac{1}{(1 + \bar{N}_s)^7} \left(1 + 7 \frac{\bar{N}_s}{1 + \bar{N}_s} + 28 \frac{N_s^2}{(1 + \bar{N}_s)^2} \right)$$

The solution to this equation, obtained by the use of an electronic computer, is

$$\bar{N}_s = 3.19$$

Unclassified

Security Classification

DOCUMENT CONTROL DATA - R&D

(Security classification of title, body of abstract and indexing annotation must be entered when the overall report is classified)

1. ORIGINATING ACTIVITY (Corporate author) EG&G, Inc. Crosby Drive Bedford, Massachusetts	2a. REPORT SECURITY CLASSIFICATION Unclassified 2b. GROUP

3. REPORT TITLE

STUDY OF A MULTI-PULSE LASER RANGE FINDER

4. DESCRIPTIVE NOTES (Type of report and inclusive dates)

Scientific Report (Interim)

5. AUTHOR(S) (Last name, first name, initial)

Ackerman, Sumner (NMI)
Morrison, Thomas S.

6. REPORT DATE	7a. TOTAL NO. OF PAGES	7b. NO. OF REFS
20 October 1966	54	9

8a. CONTRACT OR GRANT NO.	9a. ORIGINATOR'S REPORT NUMBER(S)
AF 19(628)-5516 b. PROJECT NO. and Task No. 7600-06 c. Element No. 62405394 d. Sub-Element No. 681000	EG&G Report No. B-3434 Scientific Report No. 2 9b. OTHER REPORT NO(S) (Any other numbers that may be assigned this report) AFCRL-66-755

10. AVAILABILITY/LIMITATION NOTICES

Distribution of this document is unlimited.

11. SUPPLEMENTARY NOTES	12. SPONSORING MILITARY ACTIVITY
	Hq. AFCRL, OAR (CRJ) United States Air Force 01730 L. G. Hanscom Field, Bedford, Mass.

13. ABSTRACT

A programmed multi-pulse optical radar range finder is analyzed. An experimental multi-pulse laser has been developed and its characteristics are described.

If the target is optically "smooth," or is well resolved by the receiver, the multi-pulse range finder has an effective power gain slightly less than its output energy gain when the noise level is low and the detection probability is high. The useful energy gain of a ruby laser due to multi-pulsing was experimentally measured as about 8 dB.

Under the conditions of geodetic satellite ranging, the target is generally optically "rough" in the extreme; then the multi-pulse range finder has a power gain of from 10 dB to over 25 dB, depending on the relative transmitter efficiencies and the acceptable detection probability. This significant increase in the advantage of the multi-pulse system results from the detection statistics that are valid when signal scintillation due to the target is present.

DD FORM 1 JAN 64 1473

Unclassified

Security Classification

14. KEY WORDS	LINK A		LINK B		LINK C	
	ROLE	WT	ROLE	WT	ROLE	WT
Lasers Geodesy Satellites Illuminators						

INSTRUCTIONS

1. ORIGINATING ACTIVITY: Enter the name and address of the contractor, subcontractor, grantee, Department of Defense activity or other organization *(corporate author)* issuing the report.

2a. REPORT SECURITY CLASSIFICATION: Enter the overall security classification of the report. Indicate whether "Restricted Data" is included. Marking is to be in accordance with appropriate security regulations.

2b. GROUP: Automatic downgrading is specified in DoD Directive 5200.10 and Armed Forces Industrial Manual. Enter the group number. Also, when applicable, show that optional markings have been used for Group 3 and Group 4 as authorized.

3. REPORT TITLE: Enter the complete report title in all capital letters. Titles in all cases should be unclassified. If a meaningful title cannot be selected without classification, show title classification in all capitals in parenthesis immediately following the title.

4. DESCRIPTIVE NOTES: If appropriate, enter the type of report, e.g., interim, progress, summary, annual, or final. Give the inclusive dates when a specific reporting period is covered.

5. AUTHOR(S): Enter the name(s) of author(s) as shown on or in the report. Enter last name, first name, middle initial. If military, show rank and branch of service. The name of the principal author is an absolute minimum requirement.

6. REPORT DATE: Enter the date of the report as day, month, year, or month, year. If more than one date appears on the report, use date of publication.

7a. TOTAL NUMBER OF PAGES: The total page count should follow normal pagination procedures, i.e., enter the number of pages containing information.

7b. NUMBER OF REFERENCES: Enter the total number of references cited in the report.

8a. CONTRACT OR GRANT NUMBER: If appropriate, enter the applicable number of the contract or grant under which the report was written.

8b, &c, & 8d. PROJECT NUMBER: Enter the appropriate military department identification, such as project number, subproject number, system numbers, task number, etc.

9a. ORIGINATOR'S REPORT NUMBER(S): Enter the official report number by which the document will be identified and controlled by the originating activity. This number must be unique to this report.

9b. OTHER REPORT NUMBER(S): If the report has been assigned any other report numbers *(either by the originator or by the sponsor)*, also enter this number(s).

10. AVAILABILITY/LIMITATION NOTICES: Enter any limitations on further dissemination of the report, other than those imposed by security classification, using standard statements such as:

(1) "Qualified requesters may obtain copies of this report from DDC."

(2) "Foreign announcement and dissemination of this report by DDC is not authorized."

(3) "U. S. Government agencies may obtain copies of this report directly from DDC. Other qualified DDC users shall request through _____."

(4) "U. S. military agencies may obtain copies of this report directly from DDC. Other qualified users shall request through _____."

(5) "All distribution of this report is controlled. Qualified DDC users shall request through _____."

If the report has been furnished to the Office of Technical Services, Department of Commerce, for sale to the public, indicate this fact and enter the price, if known.

11. SUPPLEMENTARY NOTES: Use for additional explanatory notes.

12. SPONSORING MILITARY ACTIVITY: Enter the name of the departmental project office or laboratory sponsoring *(paying for)* the research and development. Include address.

13. ABSTRACT: Enter an abstract giving a brief and factual summary of the document indicative of the report, even though it may also appear elsewhere in the body of the technical report. If additional space is required, a continuation sheet shall be attached.

It is highly desirable that the abstract of classified reports be unclassified. Each paragraph of the abstract shall end with an indication of the military security classification of the information in the paragraph, represented as *(TS)*, *(S)*, *(C)*, or *(U)*.

There is no limitation on the length of the abstract. However, the suggested length is from 150 to 225 words.

14. KEY WORDS: Key words are technically meaningful terms or short phrases that characterize a report and may be used as index entries for cataloging the report. Key words must be selected so that no security classification is required. Identifiers, such as equipment model designation, trade name, military project code name, geographic location, may be used as key words but will be followed by an indication of technical context. The assignment of links, rules, and weights is optional.